

Article

Testosterone Reduces Myelin Abnormalities in the Wobbler Mouse Model of Amyotrophic Lateral Sclerosis

Ivan J. Esperante ¹, Maria Meyer ¹, Carolina Banzan ¹, Maria Sol Kruse ², Analia Lima ¹, Paulina Roig ¹, Rachida Guennoun ³, Michael Schumacher ³, Alejandro F. De Nicola ^{1,4}
and Maria Claudia Gonzalez Deniselle ^{1,5,*}

- ¹ Laboratory of Neuroendocrine Biochemistry, Instituto de Biología y Medicina Experimental, CONICET, Buenos Aires 1428, Argentina; esperanteivan@gmail.com (I.J.E.); mariameyer1981@gmail.com (M.M.); c.banzan@gmail.com (C.B.); alejandrodnicola@gmail.com (A.F.D.N.)
- ² Laboratory of Neurobiology, Instituto de Biología y Medicina Experimental, CONICET, Buenos Aires 1428, Argentina; sol.kruse@conicet.gov.ar
- ³ U1195 INSERM and University Paris Sud: “Neuroprotective, Neuroregenerative and Remyelinating Small Molecules”, 94276 Kremlin-Bicêtre, France; rachida.guennoun@inserm.fr (R.G.); michael.schumacher@inserm.fr (M.S.)
- ⁴ Departamento de Bioquímica Humana, Facultad de Medicina, Universidad de Buenos Aires, Buenos Aires 1121, Argentina
- ⁵ Departamento de Ciencias Fisiológicas, UA1, Facultad de Medicina, Universidad de Buenos Aires, Buenos Aires 1121, Argentina
- * Correspondence: mcgonzalez@fmed.uba.ar

Abstract: Amyotrophic lateral sclerosis (ALS) is a fatal motoneuron degenerative disease that is associated with demyelination. The *Wobbler* (*WR*) mouse exhibits motoneuron degeneration, gliosis and myelin deterioration in the cervical spinal cord. Since male *WR*s display low testosterone (T) levels in the nervous system, we investigated if T modified myelin-relative parameters in *WR*s in the absence or presence of the aromatase inhibitor, anastrozole (A). We studied myelin by using luxol-fast-blue (LFB) staining, semithin sections, electron microscopy and myelin protein expression, density of IBA1⁺ microglia and mRNA expression of inflammatory factors, and the glutamatergic parameters glutamine synthetase (GS) and the transporter GLT1. Controls and *WR* + T showed higher LFB, MBP and PLP staining, lower g-ratios and compact myelin than *WR*s and *WR* + T + A, and groups showing the rupture of myelin lamellae. *WR*s showed increased IBA1⁺ cells and mRNA for CD11b and inflammatory factors (IL-18, TLR4, TNF α R₁ and P₂Y₁₂R) vs. controls or *WR* + T. IBA1⁺ cells, and CD11b were not reduced in *WR* + T + A, but inflammatory factors’ mRNA remained low. A reduction of GS⁺ cells and GLT-1 immunoreactivity was observed in *WR*s and *WR* + T + A vs. controls and *WR* + T. Clinically, *WR* + T but not *WR* + T + A showed enhanced muscle mass, grip strength and reduced paw abnormalities. Therefore, T effects involve myelin protection, a finding of potential clinical translation.

Keywords: myelin; testosterone; androgens; aromatase; anastrozole; ALS; Wobbler mouse



Citation: Esperante, I.J.; Meyer, M.; Banzan, C.; Kruse, M.S.; Lima, A.; Roig, P.; Guennoun, R.; Schumacher, M.; De Nicola, A.F.; Gonzalez Deniselle, M.C. Testosterone Reduces Myelin Abnormalities in the Wobbler Mouse Model of Amyotrophic Lateral Sclerosis. *Biomolecules* **2024**, *14*, 428. <https://doi.org/10.3390/biom14040428>

Academic Editor: Roberto Cosimo Melcangi

Received: 6 December 2023

Revised: 22 March 2024

Accepted: 25 March 2024

Published: 1 April 2024



Copyright: © 2024 by the authors. Licensee MDPI, Basel, Switzerland. This article is an open access article distributed under the terms and conditions of the Creative Commons Attribution (CC BY) license (<https://creativecommons.org/licenses/by/4.0/>).

1. Introduction

Myelin disorders are present in common damage to myelin sheaths and to axons in the brain and/or spinal cord. The most frequent disease in this group is Multiple Sclerosis (MS) considered to be of primary autoimmune and inflammatory origin although some variants suggest primary neurodegeneration [1,2]. Although amyotrophic lateral sclerosis (ALS) is not categorized as a demyelinating disease, it shows white matter demyelination. First described by Charcot in 1869, it is characterized by the death of motoneurons in the ventral horn and/or medulla oblongata and axonal loss in the lateral columns of the spinal cord, which show a “sclerotic” appearance caused by damage, loss and scarring of the myelin sheaths [3–5]. Therefore, therapies directed to preserve myelin or remyelinate axons

should be considered for the treatment of ALS neuropathology, in addition to therapies aiming to protect motoneurons.

Interestingly, a dysfunctional endocrine system is present in ALS patients, resulting in increases of circulating cortisol and progesterone [6]. Working with the *Wobbler* (*WR*) mouse mutant [4], a model of human motoneuron diseases such as ALS, we have shown protective effects of progesterone, its metabolite allopregnanolone and the synthetic progestin, Nestorone, for damaged motoneurons. These steroids decrease oxidative stress, excitotoxicity, neuroinflammation and death-related molecules, but increase trophic factors and prevent hyperactivation of microglia and astrocytes [7,8]. In fact, inflammation of the spinal cord appears in the *WR* mouse early after birth, suggesting that proinflammatory factors play an important part in neuronal and myelin damage [9]. *WR* mice also show a pronounced hypogonadism, infertility and low levels of testosterone (T) in the brain, spinal cord and blood [10–12]. Interestingly, the neuropathology of *WR* mice bears striking similarities to that of the *SOD1*^{G93A} rat model of familial ALS, including massive myelin degeneration in the spinal cord [13].

In addition to the mentioned effects of progestins, androgens also show protective effects in the nervous system. Androgens prevent neuronal death caused by the activation of astrocytes and microglia after injury, glucose deprivation and excitotoxicity [14]. In addition, they stimulate neuronal differentiation and neurite outgrowth and inhibit oxidative stress due to mitochondrial dysfunction [15,16]. Thus, published evidence supports the anti-inflammatory, immunomodulatory and beneficial neuronal effects of androgens away from classical reproductive effects.

Regarding androgen effects on axons, Pesaresi et al. demonstrate robust sex differences in the g-ratio, an index of optimal axonal myelination, with males showing higher values than female animals. The increased g-ratio in males depends on higher levels of axon diameter that are not accompanied by an increase in the thickness of the myelin sheaths [17]. The beneficial properties of androgens also apply to the genesis of myelin and myelin regeneration. Hussein et al. (2013) have shown that androgen exposure improves remyelination in the corpus callosum after prolonged cuprizone-induced demyelination and in cultured cerebellar slices after acute lyssolecithin-induced demyelination [18]. Ghomari et al. (2020) have recently summarized the regenerative potential of T under the same conditions and also in lyssolecithin-induced demyelination and experimental autoimmune encephalomyelitis [19,20]. Both the androgen receptor (AR) and T aromatization into estrogens are considered important players of the remyelinating effects of androgen [15].

In humans with ALS, Weinert hypothesized that the disease may be caused by the lack or dysfunction of AR in motoneurons [21]. In an experimental model of familial ALS, the synthetic androgen, nandrolone, enhances neuromuscular function and preserves mitochondrial morphology [22] although opposite effects have also been reported [23]. It has been postulated that androgen protective effects on neurons may be due to crosstalk of AR with insulin growth factor1, although this interaction could obscure a direct participation of androgen effects [24]. In humans with MS and mice with experimental demyelination, Zahaf et al. (2023) have shown that androgens synergize with estrogens to recruit oligodendrocyte precursors to demyelinating lesions and that there are specific effects of androgens in the response of glial cells to myelin loss [25]. Additional studies reporting androgen effects on peripheral nerves which originated in Melcangi's laboratory described androgen protection of peripheral myelin containing the peripheral glycoprotein P0 and the peripheral myelin protein 22 (PMP22) from damage inflicted by injury, aging and diabetes [26–28]. Therefore, both peripheral as well as central myelin proteins are regulated after treatment by T or its metabolites.

Former work from our laboratory has demonstrated several T effects in the *WR* mouse. Thus, treatment with T increases the enzyme, choline acetyltransferase, in motoneurons, decreases motoneuron vacuolation (a hallmark of the disease), decreases astrogliosis, microgliosis, oxidative and nitrosative stress, reduces proinflammatory factors and improves motor behavior and paw atrophy [29]. Thus, in the former study, we focused on androgen

protective effects on spinal cord motoneurons and on reduction in reactive glial cells. In the present work, we studied several myelin-related parameters in *WR* mice with or without T treatment. To this end, we performed quantitative histochemistry of whole myelin, electron microscopy to assess myelin compaction and expression of myelin proteins. We also measured inflammatory mediators and molecules of the glutamate circuit that may impair myelination. The role of T-derived estrogens on myelination was also analyzed by exposing T-treated *WR* mice to the aromatase inhibitor, anastrozole (A).

2. Materials and Methods

2.1. Experimental Animals and Ethical Statement

Control and *WR* mice on an *NFR/NFR* background were raised at the animal room facilities of the Instituto de Biología y Medicina Experimental. Two groups were identified by genotyping analysis, i.e., wild-type male control mice (*NFR/NFR*) and male *WR* mice (*wr/wr*) [11]. Mice were kept under standard conditions, i.e., controlled humidity and temperature (22 °C), lights on from 07:00 am to 07.00 pm and fed standard mice chow ad libitum. Two-month-old *WR*s were used at the symptomatic stage which showed tremor, flexion of proximal limbs, ambulatory difficulty, diminished muscle strength and lighter body weight compared to control mice [30]. *WR* mice sacrificed at this stage show about 25% vacuolated motoneurons, a hallmark of this disease. Sample size was calculated taking into account our previous experience depending on each technique and considering a confidence interval of 95% and a medium significant size effect [7,31]. The results shown correspond to the most representative experiment from 2 experiments performed at different times. In addition, astrogliosis and microgliosis were detected by staining for cell specific markers in both gray and white matters of the cervical spinal cord [32]. All procedures reported in this paper followed the guide for the Care and Use of Laboratory Animals (NIH Guide, Instituto de Biología y Medicina Experimental Assurance Certificate #A5072-01) and were approved by the Institute's Animal Care and Use Committee on 23 July 2021. The experiments are reported in accordance with the ARRIVE guidelines (www.nc3rs.org.uk).

2.2. Treatment with Testosterone and Anastrozole, an Aromatase Inhibitor

Male mice were randomly and blindly assigned to the treatment groups. In order to analyze the effect of androgen treatment and the cotreatment of T plus the aromatase inhibitor, A, in control mice, we evaluated the effect of T or T + A treatment in male controls (*NFR/NFR*) on body weight progression and the size of seminal vesicles. As shown previously, controls + T-treated mice [29] show no differences compared to T-free controls. A similar response was found in controls + T + A-treated mice. Therefore, the following experimental groups were prepared: (1) control (CTL; n = 15), (2) *WR* (n = 15), (3) *WR* + T (n = 15), (4) *WR* + T + A (n = 15). Steroid delivery was performed by implantation of silastic tubes (Down Corning) filled with crystalline T (Sigma-Aldrich, St Louis, MO, USA) under the skin of the neck. Tubes measured 1.57 mm in inner diameter, 2.41 mm in outer diameter and 10 mm in length. Before s.c. implantation, tubes were immersed in 70% ethanol and then washed in sterile 0.9% NaCl solution. Silastic tubes were implanted in mice anesthetized with isoflurane (induction 4%; maintenance 1.5%; BAXTER Healthcare Corp., Deerfield, IL, USA) and remained in place for 60 days. The hormone delivery method produces physiological levels of T for at least 60 days as determined by gas chromatography/mass spectrometry in male mice [18,29] and promotes myelin formation in both brain and spinal cord in a mouse demyelination model [19]. Control and *WR*s not treated with T received s.c. empty silastic tubes for 60 days.

The aromatase inhibitor, A (gift from Gador Labs, Buenos Aires, Argentina) was dissolved in 10% dimethylsulfoxide (DMSO) and introduced into Alzet osmotic micropumps (model 1004-Alzet, Cupertino, CA, USA) showing a delivery rate of 1 mg/kg/day. Micropumps were implanted s.c. starting 1 week before T treatment and remained in place for

28 days, the period during which the delivery lasts. Then, two micropumps were reimplanted consecutively to complete the time of treatment (Figure 1).

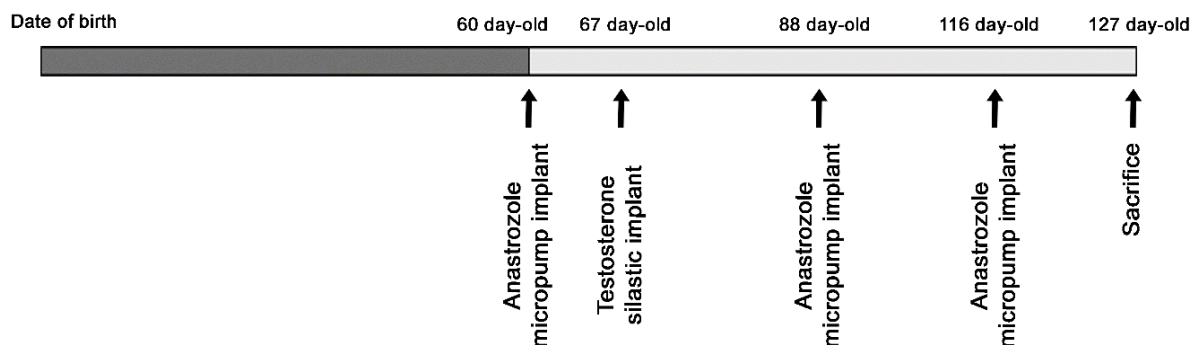


Figure 1. Time protocol for testosterone and anastrozole treatments in male Wobbler mice. Animals were implanted with a silastic tube filled with T at 67 days of age or a silastic tube filled with T at 67 days of age plus a micropump filled with anastrozole at 60, 88 and 116 days of age. Mice were killed at 127 days of age.

2.3. Semithin Sections and Electron Microscopy Studies

Sixty days after silastic tube implantation, 12 mice (controls $n = 3$, untreated WRs $n = 3$, WR + T $n = 3$ or WR + T + A $n = 3$) were anesthetized with a mixture of 6 mg/kg xylazine (Bayer, Argentina) and 75 mg/kg ketamine (Holliday-Scott, Béccar, Argentina) and intracardially perfused with ice-cold 4% paraformaldehyde in 0.1 M phosphate buffer pH 7.4 for electron microscopy. The cervical region of the spinal cord was dissected, the ventral region was cut into 2–3 mm length sections and immersed for 2 h in glutaraldehyde 2.5% in 0.1 M phosphate buffer at a pH of 7.4. After washing in the same buffer solution, sections containing the ventrolateral funiculus were postfixed for 60 min in 1% OsO₄ in 0.1 M phosphate buffer at a pH of 7.4. A final staining step was performed with 1% uranyl acetate. Afterwards, tissue sections were dehydrated and flat-embedded in Durcupan (Fluka Chem. AG, Göteborg, Sweden) for 72 h at 60 °C. Semithin (0.5 µm) and ultrathin sections (60–70 nm) were obtained using an ultramicrotome (Reichert Jung Ultracut E). Ultrathin sections were stained with lead citrate and examined at several magnifications (12,000×, 50,000× and 250,000×, respectively). Images were photographed using a Gatan W 10,000 camera connected to a Zeiss 109 electron microscope (Oberkochen, Germany). Sectioning and staining procedures were carried out at the Dept. of Histology, Faculty of Medicine, University of Buenos Aires. In addition to electron microscopy, we analyzed the density and morphological appearance of axons in the 4 experimental groups. For this purpose, semithin sections were stained with 2% toluidine blue for light microscopy observations and quantitation of the myelin thickness/axon diameter ratio [33,34]. G-ratios are presented as the axon diameter/total diameter of the axon plus the myelin sheath. Axon diameter and myelin thickness were calculated from the measured area based on the assumption of circularity using Fiji/ImageJ v1.52a ($\text{diameter} = 2 \times \sqrt{[\text{area}/\pi]}$), with a minimum of 100 axons analyzed per animal (3 animals/group). Images of semithin sections were acquired using an Axiophot Zeiss light microscope and mentioned parameters were measured using a Fiji through the semi-automated quantification of axon diameters and g-ratio via MyelTracer software v1.3.1 [34]. As an additional measure, we conducted correlative analysis of myelin thickness (in µm) vs. axon diameter (in µm) and the differences between slopes were analyzed according to Dillenburg et al. [35].

2.4. Samples for Histological and Immunohistological Analyses

Anesthetized mice were intracardially perfused with ice-cold 4% paraformaldehyde (PFA) in 0.1 M sodium phosphate buffer at a pH of 7.4. Cervical spinal cords were dissected and post-fixed in the same fixative for 2.5 h. Then, C₂–C₄ segments were embedded in paraffin or C₄–C₆ segments were frozen on dry ice after cryoprotection in 20% sucrose

overnight. Sections measuring 5 or 16 μm were cut using a microtome or a cryostat, respectively, and laid on microscope slides.

2.4.1. Luxol Fast Blue (LFB) Staining of Whole Myelin

LFB staining was carried out according to Kim et al., 2006 [36]. Briefly, 5 μm paraffin sections were treated with 95% ethanol and left in LFB solution (0.1 g LFB, 0.5 ml 10% acetic acid, 95% ethanol to 100 mL) at 60 °C for 18 h. After several washes, sections were immersed in lithium carbonate, then 70% ethanol, rinsed in distilled water, dried and mounted with Permount. The percentage of LFB staining area of the ventrolateral funiculus above an established threshold was determined using computerized image analysis as described before [37].

2.4.2. Immunohistochemistry of Myelin Basic Protein (MBP) and Proteolipid Protein (PLP)

Paraffin sections measuring 5 μm from cervical spinal cords of the different groups of mice were deparaffinized and treated with 0.3% hydrogen peroxide in methanol for 30 min to block endogenous peroxidase. Immunocytochemistry was carried out using two different primary antibodies diluted in PBS containing 1% goat serum: a rabbit anti-MBP primary antibody (1:500, Code AO623, Dako Cytomation, Carpinteria, CA, USA) and rat anti-PLP AA3 antibody (1:250, Millipore Sigma-Aldrich, St Louis, MO, USA). After overnight incubation at 4 °C and several washes with PBS, sections were incubated with either a 1/200 dilution of a biotinylated goat anti-rabbit IgG secondary antibody (Vector Labs, Newark, CA, USA) for 1 h at 22 °C, then with avidin-biotin-peroxidase (ABC) complex for 30 min (ABC kit Vector Labs, Newark, CA, USA) and revealed with 0.5 mg/mL diaminobenzidine tetrachloride (Sigma-Aldrich, St Louis, MO, USA) in the presence of 0.01% H_2O_2 for 7 min in the dark. The sections were given a final rinse in PBS, dehydrated in graded ethanol and xylene, and mounted with Permount [38].

For quantitative evaluation, MBP or PLP immunoreactive areas were delimited in the ventrolateral funiculus of the cervical spinal cord via computerized image analysis using Optimas VI software v6.5 [37]. The percentage of immunoreactive MBP or PLP area of each spinal cord section was quantified and expressed as a percentage of the total surface area of white matter sampled [37]. For quantitation of changes, comparative sections of the 4 experimental groups were averaged to obtain an independent figure for each animal ($n = 4\text{--}8$ animals per experimental group).

2.4.3. Immunohistochemical Analysis of Glutamine Synthetase (GS) and Its Colocalization with Glial Markers

Literature data support that both astrocytes and oligodendrocytes express GS [39,40]. To determine the effects of T treatment on GS protein expression and its localization, we investigated the density of GS immunostained cells/unit area (A) and also performed double labeled colocalization of GS with the astrocyte marker, GFAP, with the microglial marker IBA1 and with the oligodendrocyte marker CNPase (B). (A) For quantitation of GS⁺ cells, 5 μm paraffin sections from cervical spinal cord were blocked with mouse IgG blocking reagent (Vector M.O.M. Immunodetection Kit) and then incubated with a 1/200 dilution of monoclonal mouse anti-GS (BD Biosciences Cat.# 610517, RRID:AB_397879). We then used a 1/200 dilution of a goat antimouse biotinylated IgG (Vector Labs, Newark, CA, USA) and processed it according to the instructions of the ABC kit (Vector Labs, Newark, CA, USA). The peroxidase activity was revealed using diaminobenzidine tetrachloride (DAB, 0.25 mg/mL, SIGMA, St. Louis, MO, USA) in 0.01% H_2O_2 for 7 min in the dark. After a final rinse in PBS, sections were dehydrated in ethanol and xylene, and covered with mounting media (Permount).

(B) For astrocyte colocalization, after GS immunostaining revealed with a secondary donkey anti-mouse Alexa Red 555 (GS), a polyclonal rabbit anti-GFAP (1:250 dilution, Dako, Glostrup, Denmark) was incubated and, after several washes in PBS, followed by a secondary donkey anti-rabbit Alexa Green 488. To determine microglial colocalization,

16 μm cryostat sections were used for GS immunostaining, followed by a polyclonal rabbit anti-IBA1 (1/1000 dilution, Wako, Richmond, VA, USA) antibody for 3 days that was revealed with a secondary donkey anti-rabbit Alexa 647 antibody. For oligodendrocyte colocalization, paraffin sections subjected to antigen retrieval with HCl and boric acid followed by citrate buffer (pH = 6) were incubated with the rabbit polyclonal antibody, anti-CNPase (1/200, Sigma-Aldrich, St Louis, MO, USA) for 2 days at 4 °C followed by incubation with a secondary donkey anti-rabbit Alexa Green 488 (1/1000, Molecular Probes, Molecular Probes, Eugene, OR, USA) for 1 h at room temperature. After several washes in PBS, the sections were incubated with the GS antibody overnight at 4 °C, followed by the secondary donkey anti-mouse Alexa Red 555 antibody (1/500). Dual-labeled immunofluorescence microscopy sections for $\text{GS}^+/\text{GFAP}^+$ and $\text{GS}^+/\text{IBA1}^+$ were analyzed using an Olympus IX83 inverted microscope equipped with a disk-spinning unit (Olympus Corporation, Shinjuku City, Tokyo Japan) and images were acquired using Cell Sens Dimensions software v 1.18 from Olympus and photographed using a Hamamatsu Orca Flash 4.0 monochromatic camera (Hamamatsu Photonics K.K, Hamamatsu, Shizuoka, Japan). $\text{GS}^+/\text{CNPase}^+$ sections were visualized and images acquired using a laser scanning confocal microscope (Confocal Zeiss LSM880—Airyscan-Elyra, Zen Black 2.3) with a high-sensitivity system with a detector (Airyscan).

2.4.4. Immunohistological Localization of Glutamate Transporter-1 (GLT-1)

Paraffin sections were blocked with 1% H_2O_2 followed by 10% goat serum in PBS and exposed to a primary guinea pig GLT-1 polyclonal antibody (1:1000, cat. #AB 1783 Millipore, St Louis, MO, USA). Then, sections were incubated with a secondary anti-guinea pig antibody from Vector (1:200). Sections were then processed according to the ABC kit instructions (Vector Labs, Newark, CA, USA). GLT-1 immunoreactivity (IR) was expressed as the percentage of GLT-1 reactive area of the ventral horn.

2.4.5. Immunohistological Localization of the Oligodendrocyte Marker, CC1

Paraffin sections measuring 5 μm were blocked with 3% horse serum, and incubated with the monoclonal CC1 antibody (anti-CC1 OP80, Calbiochem, La Jolla, CA, USA) at a 1/100 dilution in 2% horse serum for 48 h at 4 °C. Then, sections were rinsed and incubated with the horse anti-mouse secondary antibody conjugated to Alexa Fluor 488 (1/500, Invitrogen, Molecular Probes, Eugene, OR, USA) for 1 h at room temperature. Next, sections were rinsed in PBS 0.1% Triton X-100 and mounted with Fluoromont G. Non-specific staining was performed in sections without the anti-CC1 primary antibody. Cell positive immunofluorescence was analyzed using an Olympus IX83 inverted microscope equipped with a disk-spinning unit (Olympus Corporation, Shinjuku City, Tokyo, Japan) and images were acquired using Cell Sens Dimensions software v1.18 from Olympus and photographed using a Hamamatsu Orca Flash 4.0 monochromatic camera (Hamamatsu Photonics K.K, Japan). The number of CC1+ cells was analyzed using the Fiji/Image J software v1.52a (NIH, MD, USA) and cell density was quantified as the number of CC1+ cells/100,000 μm^2 of the ventrolateral funiculus and expressed as a percentage of control positive cells.

2.5. Quantitative RT-PCR Analysis of mRNA Expression of Myelin Proteins, Inflammatory Factors and Glutamate Transporter

The response of WR mice spinal cord to hormone treatment and to aromatase inhibitors was also determined at the transcriptional level. We thus measured the mRNAs for (1) the myelin proteins: MBP, PLP and myelin oligodendrocyte glycoprotein (MOG), (2) proinflammatory factors: CD11b, TLR4, $\text{TNF}\alpha$ receptor₁ ($\text{TNF}\alpha\text{R}_1$), IL-18 and $\text{P}_2\text{Y}_{12}\text{R}$ and glutamate metabolism: GLT-1. All mRNA levels were measured via real-time PCR using previously published procedures [41,42]. Sequences of primers are shown in Table 1, including cyclophilin as the housekeeping gene. In brief, total RNA was extracted from cervical spinal cord with Trizol (cat.#15596026, Life Technologies-Invitrogen, Carlsbad,

CA, USA), and residual DNA was hydrolyzed with DNase1 (cat.# EC 3.1.21.1, Promega, Madison, WI, USA). For PCR amplification of DNA templates, we used a M1705 MMLV reverse transcriptase (cat# EC 2.2.2.49; Promega, Madison, WI, USA) in the presence of random hexamer primers. A real-time Step-one Plus Sequence Detection System (Applied Biosystems, Foster City, CA, USA) was used to establish gene expression profiles, and mRNA expression was analyzed using the $2^{-\Delta\Delta ct}$ method [43]. The results were expressed as fold induction over steroid untreated control *NFR/NFR* mice.

Table 1. List of sequences of forward and reverse primers.

Gene	Accession Number	Forward Primer (5→3)	Reverse Primer (5→3)
<i>MBP</i>	NM_001025100	ATCCAAGTACCTGGCCACAG	CCTGTCACCGCTAAAGAAGC
<i>PLP</i>	NM_199478	CTGGCTGAGGGCTTCTACAC	GACTGACAGGTGGTCCAGGT
<i>MOG</i>	NM_010814	AAATGGCAAGGACCAAGATG	AGCAGGTGTAGCCTCCTTCA
<i>CD11b</i>	NM_008401	AAACCACAGTCCCGCAGAGA	CGTGTTACCAGCTGGCTTA
<i>TLR4</i>	NM_021297	GGTCCTGGCTAGGACTCTGA	TCTGATCCATGCATTGGTAGGT
<i>TNFαR1</i>	NM_011609	GCTGACCCTCTGCTCTACGAA	GCCATCCACCACAGCATACA
<i>IL-18</i>	NM_008360.2	TGCCAAAAGGAAGATGATGC	ACACAAACCCTCCCCACCTA
<i>P₂Y₁₂R</i>	NM_027571.4	TTTCAGATCCGCAGTAAATCCAA	GGCTCCAGTTTAGCATCACTA
<i>GLT-1</i>	NM_001077514	CAGTGCTGGAACCTTGCCTG	GGCTATGAAGATGGCTGCCA
<i>Cyclophilin B</i>	NM_022536	GTGGCAAGATCGAAGTGGAGAAAC	TAAAAATCAGGCCTGTGGAATGTG

2.6. Clinical Assessments

The clinical effect of T alone and T + A cotreatment was studied in four different ways. First, the examination of the body weight was performed weekly. Second was by measurement of the biceps weight; third was by subjecting mice to a grip strength test [31]. In this test, empty-silastic-treated *WRs*, *WR* + T and *WR* + T + A were placed on a vertical grid and the time spent on the grid until they fell down was recorded in seconds. The time that control mice stayed on the grid could not be determined because they were able to climb to the top of the grid, while Wobblers were unable to climb against gravity. The trial was determined 3 times per animal and averaged. This determination was made weekly from the beginning (week 0: pre-treatment) until the end of the treatment (week 8). Fourth, we also evaluated the overall clinical score by assessing the grade of the deformity of the forelimbs and the eye score in the three groups of *WRs*. The atrophy of forelimbs and eye alteration were scored following Mitsumoto et al., 1994. Deformity of forelimbs included: (1) paw atrophy; (2) flexed digits; (3) flexed wrist; and (4) complete flexion of the limb over the chest. Eye condition included: 0—normal; 1—attached exudate; 2—narrowed palpebral fissure (unilateral); 3—narrowed palpebral fissures (bilateral); and 4—clogged eye (single or both) [44,45].

2.7. Statistical Analysis

All data were reported as mean \pm SD. The analysis of body weight and vertical grid was expressed as mean \pm SEM. The Shapiro–Wilk test was used to explore the normality of variables and the Levene test was used to detect homogeneous variances. Group differences were analyzed by one- or two-way ANOVA followed by the Tukey post hoc test to assess pairwise comparisons between group means. In order to analyze the progression of body weight and the performance in the vertical grid test, we analyzed data using repeated measures two-way ANOVA. Statistical analysis was performed using Prism 9 GraphPad software (San Diego, CA, USA). A *p* value < 0.05 was considered statistically significant.

3. Results

3.1. LFB Histochemistry Shows Preservation of Total Myelin in Testosterone-Treated *WR* Mice

The determination of myelin histochemical area in the ventrolateral funiculus using LFB showed significant group differences in the ANOVA test ($F_{(3,16)} = 68.34$, $p < 0.0001$). A multiple comparison test showed a 50% decrease in LFB staining in the ventrolateral

funiculus of WR spinal cord ($p < 0.0001$ vs. control mice). In T-treated WRs, % LFB reactive area was significantly increased vs. empty-silastic-treated WRs (Figure 2A, $p < 0.0001$) reaching the levels for control mice.

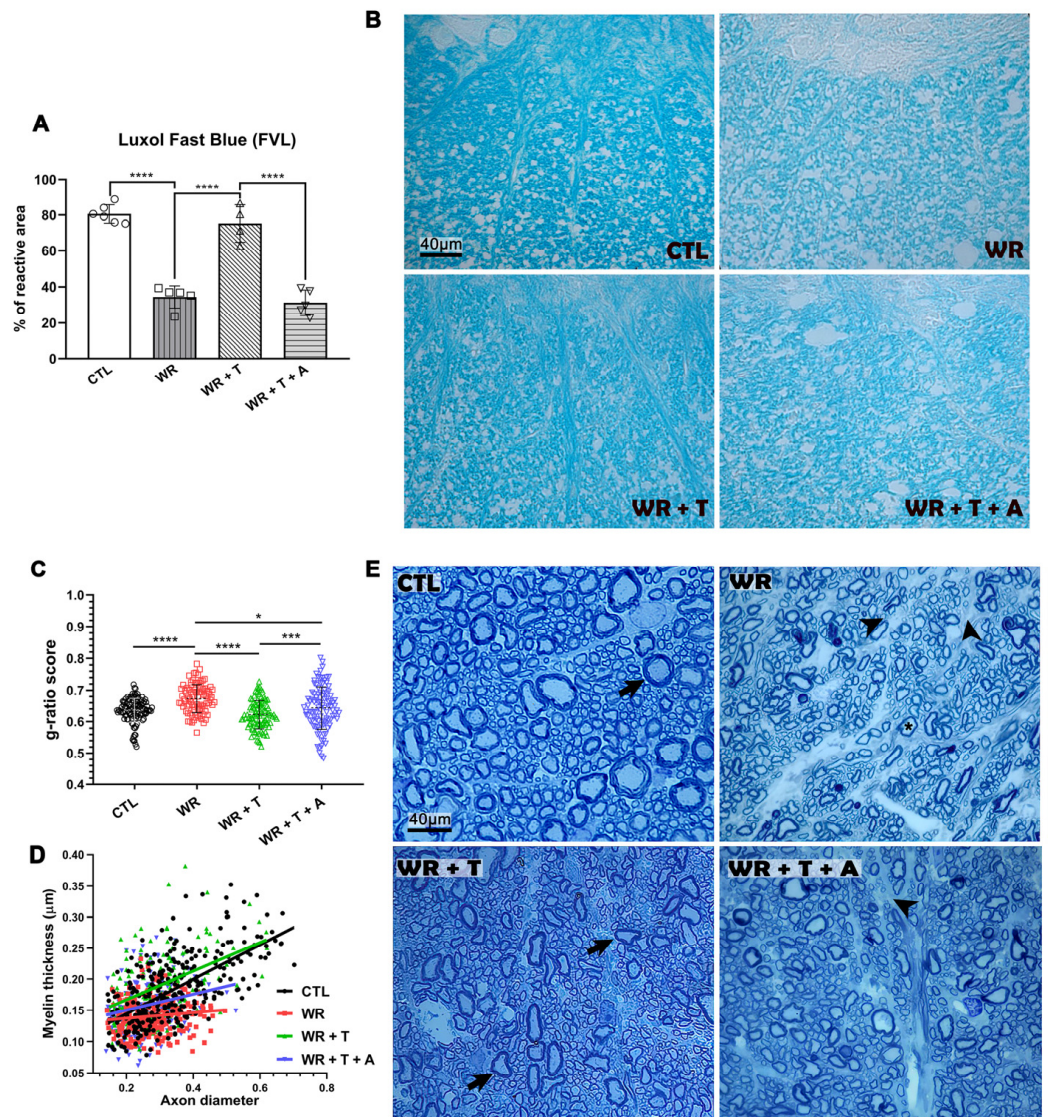


Figure 2. Effect of testosterone and anastrozole on myelination in Wobbler mice. **(A):** LFB staining of whole myelin in the spinal cord. WR mice showed decreased LFB reactive area vs. controls ($p < 0.0001$). In WR + T, LFB reactive area returned to control levels (WR + T vs. CTL, NS; WR + T vs. WR $p < 0.0001$). The WR T + A group showed a pronounced decrease in LFB reactive area ($p < 0.0001$ vs. WR + T; NS vs. WR). **(B):** Images of LFB staining in the ventrolateral funiculus of a CTL, WR, WR + T and a WR + T + A groups. Scale bar: 40 μm. **(C):** Statistical comparison of g-ratios in the four experimental groups. G-ratios were higher in WR mice vs. control mice (**** $p < 0.0001$), WR+T+A (* $p < 0.05$) and T treatment decreased this ratio vs. untreated WR mice (**** $p < 0.0001$). The graph also shows that inhibition of aromatase in the WR + T group increased the g-ratio (*** $p < 0.001$ vs. WR + T). **(D):** Plot of the relationship between the axon diameter and the myelin thickness. **(E):** Toluidine blue staining of semithin sections in the four experimental groups. Loss of myelinated axons (arrowhead) and large-caliber axons with abnormally thin myelin sheaths (asterisk) are clearly observed in the WR mouse compared to strong myelinated axons in control and WR + T (arrows). WR + T + A group showed a decreased density of myelinated axons (arrowhead). Scale bars: 40 μm. CTL: control, WR: Wobbler, T: testosterone, A: anastrozole.

To determine if estrogen synthesis plays a role in T-induced remyelination, WRs received T plus the aromatase inhibitor, A (Figure 2A). Blockage of aromatase resulted in low levels of LFB staining area ($p < 0.0001$ vs. WRs + T) suggesting that T aromatization into estrogens contributes to myelin preservation. Figure 2B shows representative images of LFB staining in the ventrolateral funiculus.

3.2. Testosterone Restores the Thickness of Myelin Sheaths in Wobbler Mice

Toluidine blue staining of semithin sections was employed to discern myelination status and calculation of myelin thickness, axon diameter and the g-ratio (i.e., the ratio of the inner to outer diameter of a myelinated axon in the four experimental groups). G-ratio is widely used as a functional and structural index of myelin sheath thickness of individual axon fibers [35]. One-way ANOVA showed significant differences between groups ($F_{(3,394)} = 16.08$, $p < 0.0001$, Figure 2C). In particular, g-ratio scores were higher in WRs vs. control mice ($p < 0.001$). Instead, T treatment of the WR mice decreased g-ratios ($p < 0.001$ vs. untreated WR) but in WR + T + A, g-ratios increased to the levels of the untreated WR group ($p < 0.001$). Changes in g-ratios, therefore, underlined once more that demyelination of the WR group was restored by T treatment, and further suggested a role of aromatase in this event. To better assess the current differences in myelin and axons in the four experimental groups, we plotted myelin thickness (in μm) vs. axon diameter (in μm) following the procedure of Dillenburg et al. 2018 [35]. The graph in Figure 2D shows that the regression line for control mice ($Y = 0.2774 \times X + 0.08884$) and for T-treated WR ($Y = 0.2302 \times X + 0.1208$) were different from zero ($p < 0.001$ for both conditions). Instead, the regression line of steroid untreated WR was not significantly different from zero ($y = 0.04479 \times X + 0.11208$, $p > 0.05$). The regression line for the WR + T + A group was also significant ($y = 0.1287 \times X + 0.11244$, $p > 0.05$) although it was shorter than the lines of the control and WR + T groups. Figure 2E shows representative images of semithin sections from the ventrolateral funiculus of a control, WR, WR + T and WR + T + A. Control axons (CTL) show a predominant round morphology with compacted, well-preserved myelin sheaths. In comparison, WR mice showed small-caliber axons with very thin myelin sheaths, suggesting demyelination. Instead, the WR + T group showed myelinated axons of several sizes suggesting partial remyelination. The T effect was in part estrogen dependent, since blockage of aromatase with A showed a coexistence of myelinated axons with demyelinated axonal profiles (WR + T + A group in Figure 2E).

3.3. Testosterone Restores Axonal Myelination in WR Mice: Analysis by Using Electron Microscopy (EM)

In the ventrolateral funiculus, control mice receiving empty silastic tubes showed thick-caliber myelinated axons, with well-compacted myelin sheaths and with a circular or elongated shape. Some mitochondrial and punctiform structures resembling microtubules were observed inside the axonal cytoskeleton (CTL-Figure 3A: low magnification, Figure 3B: high magnification, Figure 3C: inset from B). These images are in deep contrast with those from WR mice. The latter showed irregularly shaped axonal profiles, with detachment, dissolution and rupture of myelin lamellae (Figure 3D) and a few visible mitochondria and microtubules in the cytoskeleton. These images indicate axonal degeneration and demyelination (WR-Figure 3D: low magnification, Figure 3E: high magnification, Figure 3F: inset from E). In T-treated WR mice, circular and elongated axonal profiles reappear, with well-compacted myelin sheaths surrounding axons containing mitochondria (WR + T, Figure 3H). Moreover, the abundance of thinner myelinated axons in WR + T suggests reduced degeneration and enhanced remyelination (Figure 3 WR + T, G: low magnification, H: high magnification, I: inset from H). The percentage of axons with myelin abnormalities in the ventrolateral funiculus was 41.2 in WR, 24.4 in WR + T and 54.6 in WR + T + A inside an $800 \mu\text{m}^2$ field. Consistent with the results for semithin sections, androgen protective effects seemed in part to depend on estrogen synthesis. Thus, aromatase inhibition returned distorted axons, reduced myelin thickness with partial detachment and disorganization

of myelin lamellae which had an onion-like appearance when examined by using EM (*WR + T + A*, Figure 3J: low magnification, K: high magnification, L: inset from K). Still, mitochondria were visible inside these pathological axons.

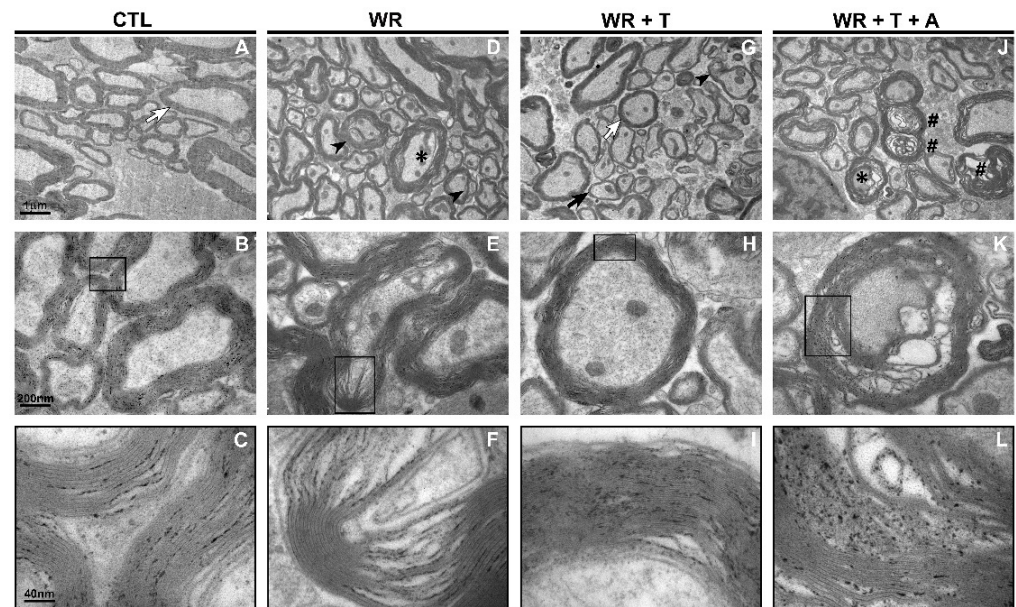


Figure 3. Effects of testosterone on axonal myelination and myelin compaction in Wobbler mice: digital Images of EM of the ventrolateral funiculus of the cervical spinal cord. (A–C): CTL mouse, (D–F): *WR* mouse, (G–I): *WR + T* mouse, (J–L): *WR + T + A* mouse. (A,D,G,J) are low power magnification images at 12,000 \times and (B,E,H,K) are high power magnification images at 50,000 \times , whereas (C,F,I,L) correspond to insets in (B,E,H,K), respectively, taken at 250,000 \times , scale bar: 40 nm. The EM photographs of CTL and *WR + T* mice showed axons surrounded by well-preserved myelin sheaths (white arrows in (A,G)). Small-caliber axons in the *WR + T* mouse suggest remyelination (black arrow, (G)) and few signs of myelin abnormalities with invagination of myelin lamellae (arrowhead, (G)). In contrast, images taken at both magnifications of untreated *WR* and *WR + T + A* mice showed irregularly shaped axons with dissolution and detachment of myelin lamellae (asterisks), invagination of myelin lamellae (arrowhead) and signs of axonal degeneration (hash symbol #). The insets in (C,I) depict the preservation of myelin sheath lamellae in the *WR + T* whereas those in (F,L) indicate myelin derangement in the *WR* and *WR + T + A* groups. Scale Bars: 1 μ m (upper), 200 nm (middle), 40 nm (bottom). CTL: control, *WR*: Wobbler, T: testosterone, A: anastrozole. EM: electron microscopy.

3.4. Testosterone Modulates the Expression of Myelin Proteins

The results obtained using LFB, semithin sections and EM indicated decreased thickness and compaction of myelin sheaths in *WR* mice. As dysregulation of myelin protein expression may compromise myelin formation and integrity, these data were complemented with assays of the expression of the major central myelin proteins MBP, PLP and MOG.

ANOVA analysis showed significant group differences in MBP mRNA ($F_{(3,21)} = 11.43$; $p < 0.001$) in the cervical spinal cord. The multiple comparison test showed similar mRNA expression between control and *WR* mice (Figure 4A). However, MBP mRNA was higher in *WR + T* vs. untreated *WRs* ($p < 0.01$) or control mice ($p < 0.001$). However, MBP mRNA levels in the *WR + T + A* group were lower than *WR* alone ($p < 0.05$) and *WR + T* ($p < 0.001$), suggesting that T effects on MBP mRNA levels were not independent from estrogen formation.

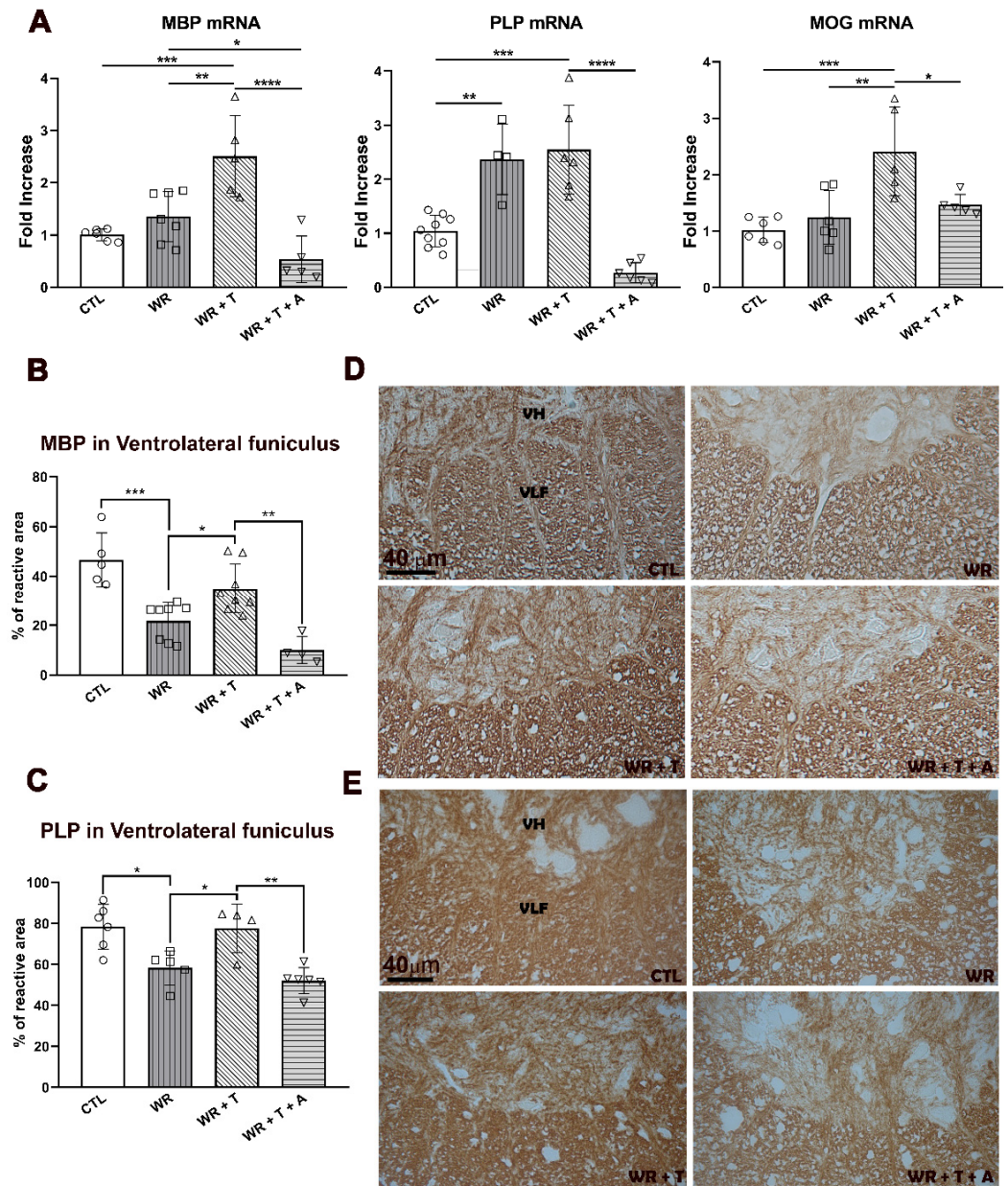


Figure 4. Effects of testosterone and anastrozole on the mRNA expression for the myelin proteins, MBP, PLP, and MOG (A) and immunoreactivity for MBP and PLP in the cervical spinal cord (B). (A) MBP mRNA (left-hand graph): CTL and WR shared similar expression levels, whereas the WR + T group showed higher values vs. control ($*** p < 0.001$) or WR alone ($** p < 0.01$). The WR + T + A group showed lower values than WR alone ($* p < 0.05$) and WR + T ($**** p < 0.0001$). PLP mRNA (middle graph): WR and WR + T groups showed increased expression vs. control ($** p < 0.01$ and $*** p < 0.001$, respectively). Aromatase inhibition (WR + T + A) produced a marked inhibition of PLP mRNA expression vs. WR + T mice ($**** p < 0.0001$). MOG mRNA (right-hand graph): CTL and WR showed similar mRNA levels whereas WR + T showed higher expression vs. control ($*** p < 0.001$) and WR ($** p < 0.01$). This stimulatory effect disappeared in the WR + T + A group ($* p < 0.05$, WR + T + A vs. WR + T). (B) The high immunoreactivity of MBP and (C) PLP in the WR + T group ($* p < 0.05$ vs. WR) was down-regulated in the ventrolateral funiculus of WR + T + A ($** p < 0.01$ in both cases). (D,E): Light microscope images of the ventrolateral funiculus show changes for MBP and PLP in the four groups of mice quantified in the graphs from (B,C), respectively. VH: ventral horn, VLF: ventrolateral funiculus, CTL: control, WR: Wobbler, T: testosterone, A: anastrozole.

The ANOVA test for PLP mRNA also showed significant group differences ($F_{(3,21)} = 11.43$; $p < 0.001$). Multiple comparisons for PLP mRNA showed a distinctive pattern. Thus, higher levels of PLP mRNA were measured in WR mice comparatively to control mice (Figure 4A, $p < 0.01$). T did not change PLP mRNA levels ($p > 0.05$ WR + T vs. WR). Furthermore, WR + T + A showed a marked reduction in PLP mRNA (Figure 4A, $p < 0.001$ vs. WR + T), implying estrogenic regulation of PLP expression. Finally, the ANOVA test also showed intergroup differences for MOG mRNA ($F_{(3,29)} = 8.271$; $p < 0.001$). In resemblance to MBP, no difference was found for MOG mRNA between control and untreated WRs, but it was significantly increased in the WR + T group ($p < 0.01$ vs. empty-silastic-treated WRs; $p < 0.001$ vs. controls). In contrast to MBP mRNA, aromatase inhibition in T treated-WR mice significantly reduced MOG mRNA (WR + T + A: $p < 0.05$ vs. WR + T, Figure 4A). In conclusion, even though mRNAs for myelin proteins were not reduced in WRs, T treatment had a stimulatory effect on both MBP and MOG mRNAs. These results suggest a possible transcriptional effect of T on MBP, and MOG but not PLP mRNA and are in consonance with steroid effects on myelin morphology.

In the ventrolateral funiculus of the white matter, WRs showed a significant reduction of MBP immunoreactive protein in comparison to controls ($p < 0.001$, Figure 4B) and to WR + T ($p < 0.05$). Furthermore, WR mice showed no difference when compared to WR + T + A mice. Similarly, PLP immunoreaction was increased in WR + T vs. WR mice (Figure 4C, $p < 0.05$ vs. WR), and remained lower in WR + T + A vs. WR + T ($p < 0.01$). Figure 4D,E show representative images corresponding to MBP and PLP immunoreactive proteins. The density of mature oligodendrocytes was analyzed following detection using immunofluorescence staining with the CC1 antibody. The ANOVA test showed significant differences between experimental groups in regard to the density of cells expressed as the percentage of control values located in the ventrolateral funiculus ($p < 0.0001$, $F = 33.86$). A significant reduction was found in WRs vs. control (mean \pm SD in WR: $61.66\% \pm 15.58$, * $p < 0.05$ vs. control: 100 ± 6.80). WR + T showed a significant increase in CC1+ cell density over WR and control values (WR + T: 162.7 ± 14.76 , **** $p < 0.0001$ vs. WR and ** $p < 0.01$ vs. controls). On the contrary, WR + T + A show similar values to WR mice (65.35 ± 19.46 , NS vs. WR, **** $p < 0.0001$ vs. WR + T and * $p < 0.05$ vs. control).

3.5. Testosterone Reduces the Activation of Microglia and the Expression of Proinflammatory Mediators in the Wobbler Spinal Cord

Proinflammatory factors produced by reactive glial cells play an important role in demyelination [46,47]. Here, we studied the expression of two markers of microglia, namely CD11b mRNA and IBA1 immunoreactive protein together with the mRNA expression of proinflammatory factors: IL-18 (an inflammatory interleukin), TLR4 (receptor for alarmins), $\text{TNF}\alpha\text{R}_1$ (a major inflammatory mediator) and the purinergic receptor ($\text{P}_2\text{Y}_{12}\text{R}$, signal for inflammation). ANOVA analysis showed significant group differences for CD11b mRNA ($F_{(3,18)} = 18.09$, $p < 0.0001$). Post hoc comparisons revealed increased mRNA expression of CD11b in WR mice ($p < 0.001$ vs. CTL), which was decreased by T administration ($p < 0.05$). The T negative effect on CD11b was blunted by aromatase inhibition ($p < 0.01$ WR + T + A vs. WR + T, Figure 5A). As shown in Figure 5B, the ventral region (ventral horn of the gray matter plus ventrolateral funiculus of the white matter) from male WR mice displayed a significantly higher density of IBA1+ cells/area in comparison to controls ($p < 0.05$). In contrast, WR + T showed reduced IBA1 immunostaining comparatively to untreated WR mice ($p < 0.01$). The density of IBA1+ cells in WR + T + A was higher than in WR + T mice ($p < 0.05$) and was similar to empty-silastic-treated WRs, suggesting a role for estrogens in the T effect. Regarding their morphology, a high percentage of IBA1+ cells displayed a reactive phenotype (Figure 5C,D: cells with ≤ 2 branches), while WR + T showed cells with a higher number of branches (≥ 3 branches, $p < 0.0001$ vs. WR), characteristic of a less reactive phenotype (Figure 5C,D). High branching was also observed in the WR + T + A group (Figure 5C, $p < 0.01$ vs. WR and Figure 5D, right-hand image).

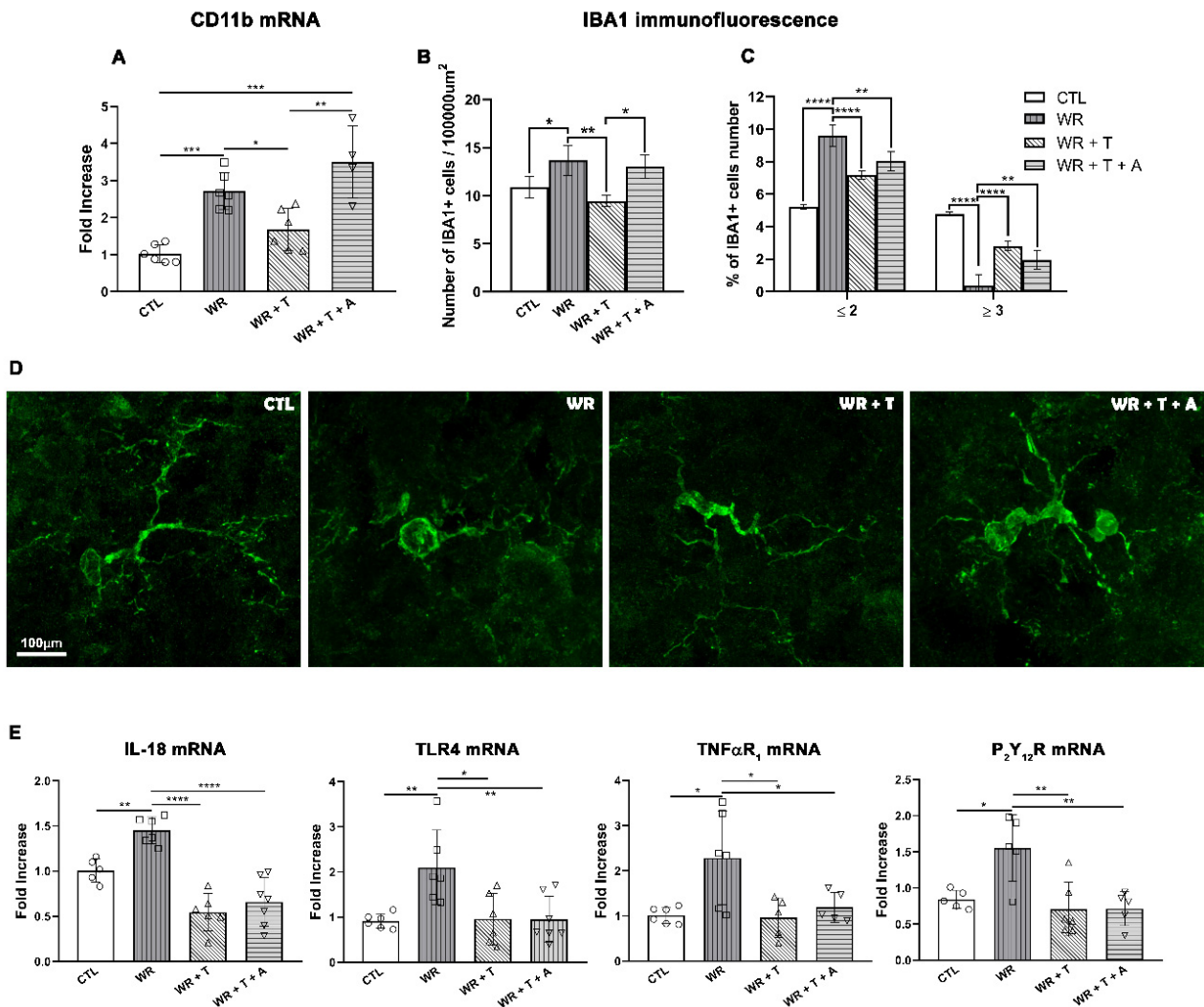


Figure 5. Effect of testosterone and anastrozole on inflammatory-related factors in Wobbler mice. (A,B) Androgen treatment reduced the high levels of *CD11b* mRNA and IBA1 cell density (expressed as number of IBA1+ cells/100,000 μm²) in WRs (*CD11b* mRNA: * $p < 0.05$; IBA1+ cell density: ** $p < 0.01$, WR + T vs. WR, respectively) and this effect was not observed in WR + T + A (*CD11b* mRNA and IBA1+ cell density: NS vs. WR) which showed higher levels of *CD11b* mRNA than CTL (** $p < 0.001$). (C) WR + T and WR + T + A showed a lower percentage of IBA1+ cells with a low number of branches (≤ 2) and increased those with ≥ 3 branches. (D) Representative images of IBA1+ cells in control, WR, WR + T and WR + T + A in the white matter of the cervical spinal cord. (E) The high levels of mRNA of inflammatory factors (*IL-18*, *TLR4*, *TNFαR₁*, *P₂Y₁₂R*) of untreated WRs were decreased in WR + T (**** $p < 0.0001$ for *IL-18*, * $p < 0.05$ for *TLR4* and *TNFαR₁* and ** $p < 0.01$ for *P₂Y₁₂R* vs. WR) or in WR + T + A (**** $p < 0.0001$ for *IL18*, ** $p < 0.01$ for *TLR4*, * $p < 0.05$ for *TNFαR₁*, ** $p < 0.01$ for *P₂Y₁₂R* vs. WR, respectively) in the whole cervical spinal cord. CTL: control, WR: Wobbler, WR + T: Wobbler + testosterone, WR + T + A: Wobbler + testosterone + anastrozole.

IL-18 mRNA expression in the cervical spinal cord showed significant group differences in the ANOVA test ($F_{(3,20)} = 24.54$, $p < 0.0001$). The post hoc test revealed that untreated WRs presented higher levels of *IL-18* mRNA than control mice ($p < 0.01$), which were decreased in WR + T ($p < 0.0001$ vs. WR). The cotreatment of WR with T + A did not modify the low levels of this interleukin comparatively to mice receiving only T (NS, WR + T vs. WR + T + A, Figure 5E). Similar results were obtained in the *TLR4* mRNA via ANOVA analysis ($F_{(3,21)} = 6.320$, $p < 0.01$). Tuckey's multiple comparison test for *TLR4* mRNA showed higher values in WR mice ($p < 0.01$ vs. control) which declined

following T treatment ($p < 0.05$ vs. WR). Similar to results with IL18 mRNA, TLR4 mRNA showed no changes in WR + T + A vs. WR + T and displayed lower levels than untreated WRs ($p < 0.01$, Figure 5E).

ANOVA analysis also showed significant group differences for TNF α R₁ mRNA ($F_{(3,18)} = 6.025$, $p < 0.001$) and for P₂Y₁₂R mRNA ($F_{(3,17)} = 7.765$, $p < 0.001$). These two inflammatory mediators showed similar expression profiles in response to the androgenic steroid or anti-aromatase treatment. As shown in Figure 5E, the mRNA of TNF α R₁ was elevated in WR mice compared to control mice ($p < 0.05$) and returned to control levels in WR + T or WR + T + A groups ($p < 0.05$). Post hoc analysis of the purinergic receptor showed increased P₂Y₁₂R mRNA in the WR group ($p < 0.05$ vs. control), which was down-regulated in both the WR + T and the WR + T + A groups ($p < 0.01$ vs. WR). Therefore, these four inflammatory mediators showed a similar expression profile: high expression in WR mice, reduction after treatment with T alone or with T plus the anti-aromatase inhibitor.

3.6. Effects of Testosterone and Anastrozole on Glutamine Synthetase in the Cervical Spinal Cord

Astrocytes and oligodendrocytes express GS, an enzyme that converts glutamate into glutamine in the CNS [40]. In particular, WR astrocytes show low expression of GS [42,48]. To study the effects of T and A on the glutamatergic system, we measured the levels of GS and the glutamate transporter GLT-1 that clears excess glutamate from synapses. In accordance with previous findings [48], WRs showed fewer GS⁺ cells/area than control mice in the ventral horn of gray matter ($p < 0.01$, Figure 6A) and the ventrolateral funiculus of white matter ($p < 0.01$, Figure 6B), while GS immunostaining returned to control levels in both regions of WR + T (ventral horn: $p < 0.001$ and ventrolateral funiculus: $p < 0.01$ vs. WRs, Figure 6A,B). However, the stimulatory effect disappeared in both regions in WR + T + A ($p < 0.001$ and $p < 0.01$ vs. WR + T, respectively, Figure 6A,B), showing similar values to empty-silastic-treated WRs. Figure 6C depicts representative images of GS immunostaining of the four experimental groups.

ANOVA analysis also showed significant group differences in the transporter GLT-1 mRNA ($F_{(3,22)} = 8.784$, $p < 0.001$). The multiple comparison test showed a significant reduction in GLT-1 mRNA in WRs bearing empty silastic tubes ($p < 0.05$ vs. control, Figure 6D). GLT-1 mRNA increased after T treatment ($p < 0.05$ vs. WRs), an effect reversed by A ($p < 0.01$ vs. WR + T, Figure 6D). Similar results were observed for GLT-1 immunoreactivity in the lamina IX of the ventral horn. WRs showed a significant reduction in the percentage of GLT-1-IR area in comparison to controls ($p < 0.01$, Figure 6E) which was increased by T treatment ($p < 0.001$ vs. WRs). However, T plus A-treated WRs showed levels of GLT-1 immunoreaction similar to those of empty-silastic-treated WRs (NS vs. WRs, $p < 0.01$ vs. WR + T, Figure 6E). Figure 6F shows the representative images of GLT-1 immunoreaction in the Lamina IX of the ventral horn.

To identify the cell type expressing GS, we performed double immunofluorescence for GS⁺/GFAP⁺ (astrocytes), GS⁺/IBA1⁺ (microglia) and GS⁺/CNPase⁺ (oligodendrocytes) in cervical spinal cord sections. In all groups, double labeled GS⁺/GFAP⁺ cells showed a low level of colocalization (2–3% of cells, arrows, Figure 7A). With regard to GFAP⁺ cells (Figure 7A, green channel), empty-silastic-treated WRs showed a high density of GFAP⁺ cells in the ventral horn in agreement with previous results [30,48,49]. WR + T revealed low levels of immunoreaction (Figure 7A) as previously shown in Lara et al., 2021 [29]. In WR + T + A, the addition of the aromatase inhibitor slightly reduced this parameter. Regarding GS⁺/IBA1⁺ colocalization, no double labeled cells were found in the four experimental groups (Figure 7B). In particular, empty-silastic-treated WRs and WR + T + A showed lower immunoreactivity for GS (red channel, Figure 7A,B) and higher immunofluorescence for IBA1 than control and WR + T groups (Figure 7B). Double immunofluorescence for GS/CNPase revealed high levels of colocalization in controls and treated or untreated WRs (Figure 7C, low magnification images). Observations made at high magnification and resolution using the high-sensitivity system with a detector

(Airyscan) showed lower immunofluorescence for both markers in WR and WR + T + A groups (Figure 7D).

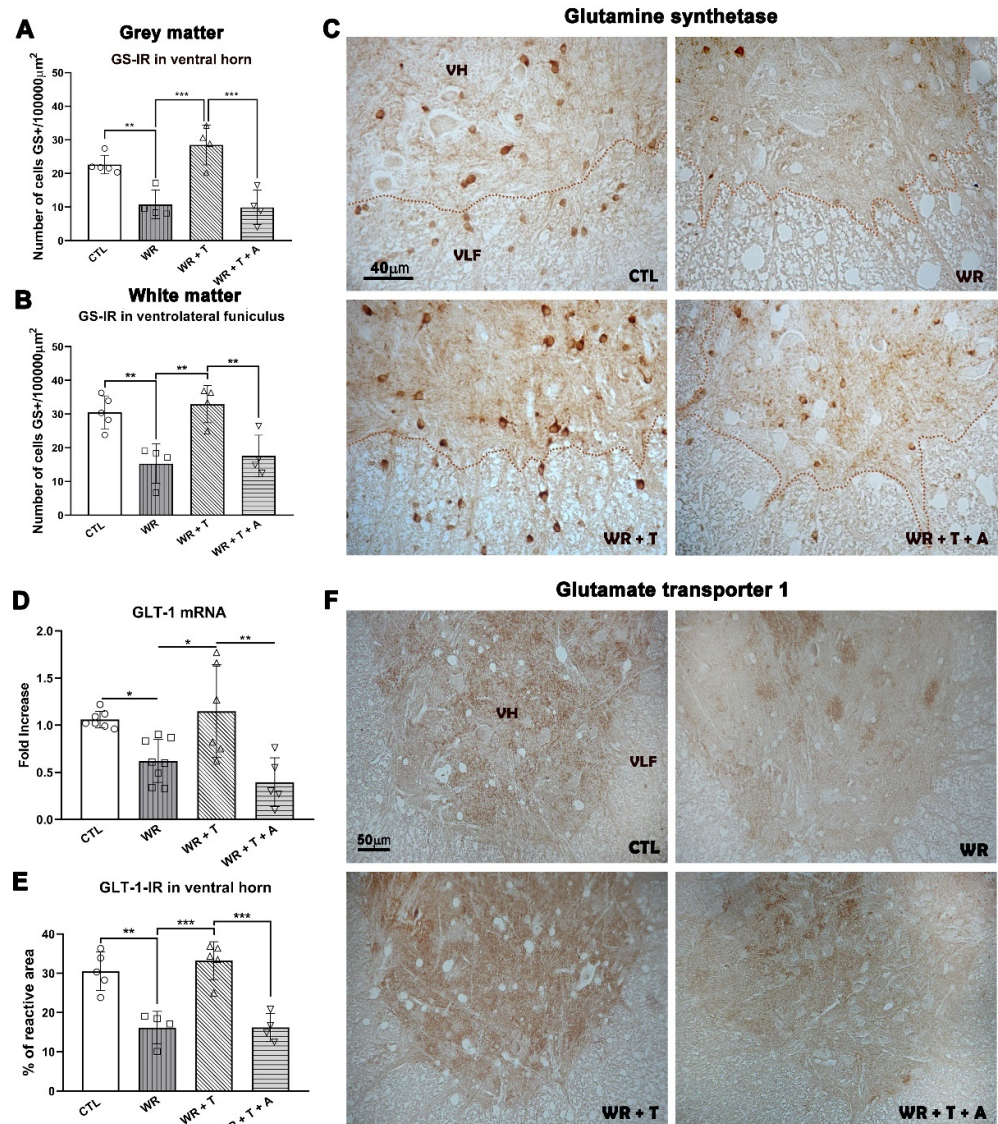


Figure 6. The low levels of GS and GLT-1 in Wobblers were up-regulated by testosterone treatment but not by cotreatment of testosterone plus the aromatase inhibitor. (A,B): The density of GS+ cells/area was low in WR and WR + T + A, but it increased in WR + T in ventral horn ((A), gray matter, *** $p < 0.001$) and ventrolateral funiculus ((B), white matter, ** $p < 0.01$). (C) Representative images of GS+ cells in gray (VH) and white matter (VLF) of the ventral region from the cervical spinal cord in the four experimental groups quantified in A and B. (D) Low expression of *GLT-1* mRNA in WR and WR + T + A compared to higher levels of *GLT-1* mRNA in WR + T. (E) Percentage of immunoreactive area was lower in the Lamina IX of WRs and WR + T + A, whereas higher percentage of immunoreactive area was shown in WR + T. (F) Representative images of GLT-1 staining in the ventral horn of the four experimental groups quantified in the graphs of (D,E). CTL: control, WR: Wobbler, WR + T: Wobbler + testosterone. WR + T + A: Wobbler + testosterone + anastrozole, GS: glutamine synthetase, GLT-1: glutamate transporter-1, VH: Ventral horn, VLF: Ventrolateral funiculus *: $p < 0.05$, ** $p < 0.01$ and *** $p < 0.001$.

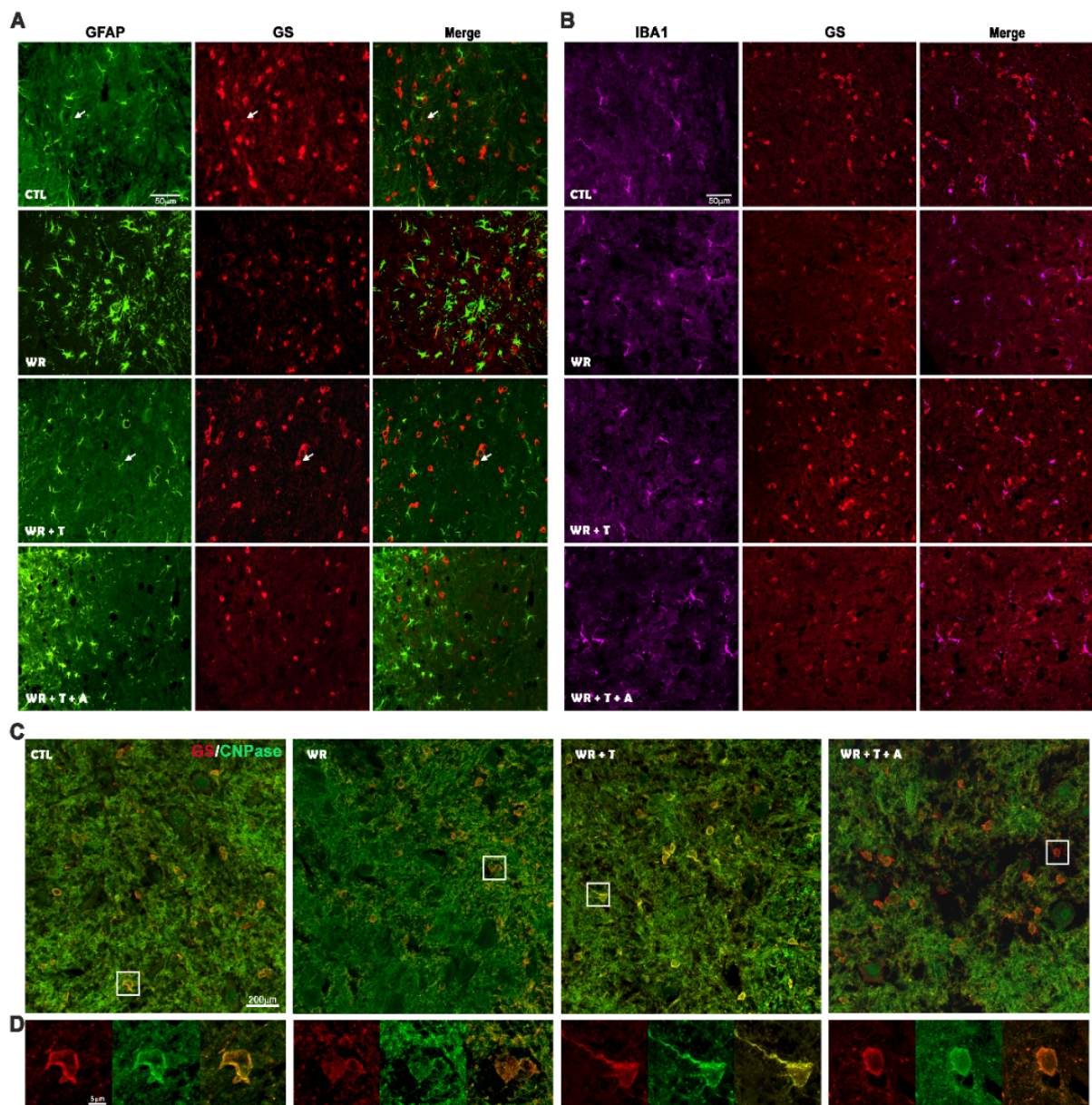


Figure 7. Representative images of double immunofluorescence for GS/GFAP (A), GS/IBA1 (B) and GS/CNPase (C,D) in the ventral horn (gray matter) of the cervical spinal cord from control, untreated WR, WR + T and WR + T + A. Arrows show cells that colocalize for GS/GFAP. The square in (C) is illustrated at high magnification in (D).

3.7. Effects of Testosterone and Anastrozole on the Biceps Weight, Body Weight, Clinical Parameters and Endocrine Glands

In addition to the T effects on myelination, glial reactivity, inflammatory markers and glutamatergic system described in WR spinal cord, chronic T administration also modified biceps weight and clinical parameters. WRs showed decreased biceps weight probably due to poor innervation from the ailing motoneurons ($p < 0.0001$ vs. control mice, Figure 8A). This effect was attenuated by T ($p < 0.001$), but the beneficial effects of T were not observed in the presence of A. These observations indicate the functional consequences of the coadministration of the male sex steroid with the aromatase inhibitor. Repeated measures two-way ANOVA and the Tukey post hoc test demonstrated that WR + T performed better in a vertical grid ($p < 0.05$, Figure 8B) whereas empty-silastic-treated WRs and those receiving T + A showed a similar performance after 8 weeks of

treatment (Figure 8B). Moreover, WR + T also showed a better clinical index score at the time of sacrifice in comparison to empty-silastic-treated WRs and WR + T + A ($p < 0.01$, Figure 8C). As expected, the body weight of controls was greater than any of the WR groups ($p < 0.0001$, Figure 8D). There was a steady increase in body weight in controls ($p < 0.001$), WRs ($p < 0.01$) and WR + T ($p < 0.001$) for the 60 days of follow-up as shown by repetitive measures two-way ANOVA ($F_{(24, 505)} = 1567$, $p < 0.05$, Figure 8D), and between day 1 and day 42 in WR + T + A ($p < 0.05$, Figure 8D).

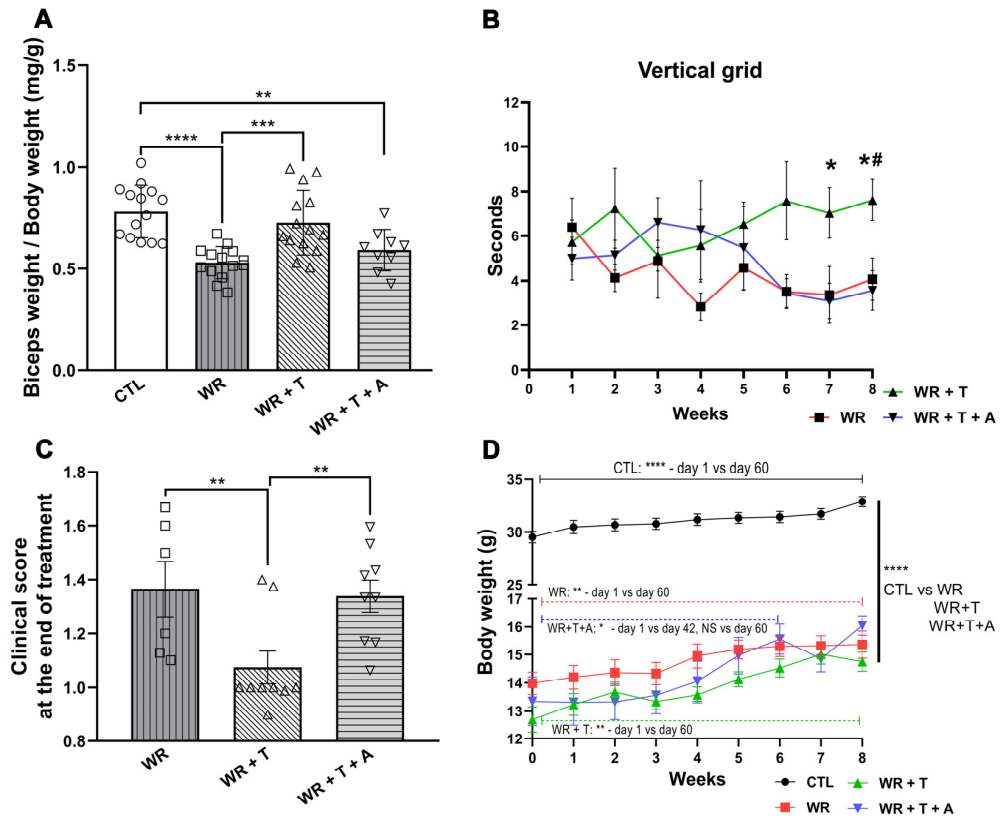


Figure 8. Increase in biceps muscle weight, vertical grid performance and body weight associated with low clinical score in WR + T but not in WR + T + A or WR. (A) Reduction of biceps weight/body weight in WRs and WR + T + A ($*** p < 0.001$, $** p < 0.01$ vs. control, respectively), but not in WR + T mice (NS vs. control, $*** p < 0.001$ vs. WR). (B) Better performance in Vertical Grid of WR + T ($* p < 0.05$ vs. WR and $\# p < 0.05$ vs. WR + T + A) and (C) lower clinical disease index score ($** p < 0.01$) vs. WRs and WR + T + A. (D) Control showed higher body weight than WR, WR + T or WR + T + A groups ($**** p < 0.0001$). Repeated measures ANOVA revealed that body weight at the end of experiment is higher than day 1 ($**** p < 0.0001$) in CTL ($** p < 0.01$) WR or WR + T, whereas WR + T + A group showed an increase between day 1 and day 42 ($* p < 0.05$) but not between day 1 and day 60. CTL: control, WR: Wobbler, WR + T: Wobbler + testosterone. WR + T + A: Wobbler + testosterone + anastrozole.

With regard to sex steroid target tissues, empty-silastic-treated WRs showed an elevation in pituitary/body weight and testis/body weight ($* p < 0.05$ and $** p < 0.01$ vs. control mice, respectively, Figure 9 A,B), without changes in seminal vesicles/body weight. WR + T showed a decreased testis size ($**** p < 0.001$ vs. WRs, Figure 9B) and a trophic effect on seminal vesicles ($**** p < 0.001$ vs. WRs, Figure 9C), without changes in the pituitary/body weight (NS vs. WRs; Figure 9A). Aromatase inhibition in WR + T + A did not change testis or seminal vesicles mass (Figure 9B,C) but significantly decreased pituitary weight/body weight (Figure 9A: $p < 0.05$ vs. WR + T). Although T-derived estrogens did not apparently play a role in the effect of T in testis or seminal vesicles, the elevation of the pituitary weight in untreated male WRs suggests the participation of endogenous estrogens in this effect.

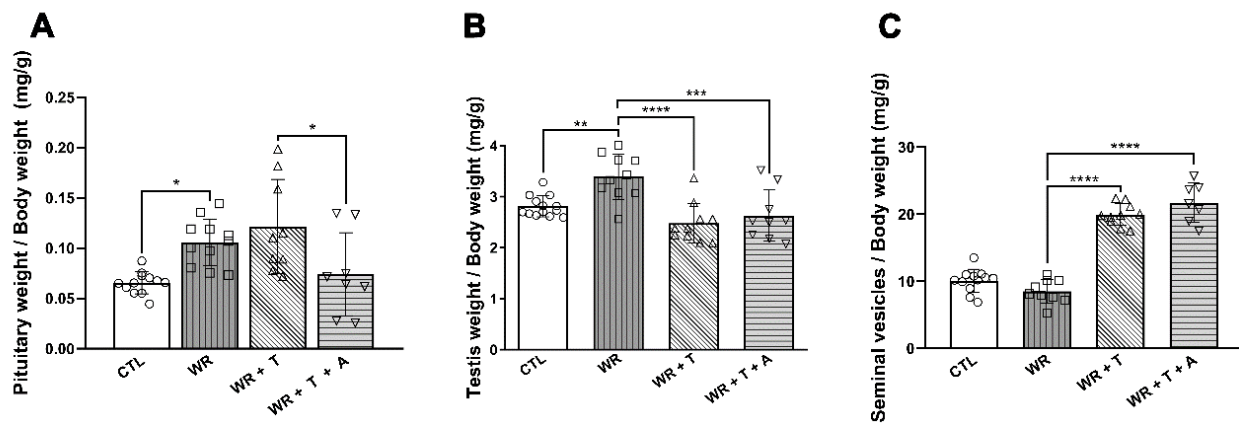


Figure 9. Increased size of the pituitary gland/body weight ((A), * $p < 0.05$) and testis/body weight in WR ((B): ** $p < 0.01$ vs. control), but only pituitary gland did not show an effect in WR + T (NS vs. WR). WR + T + A showed a reduced pituitary gland size compared to that of WR + T or WR ((A): * $p < 0.05$). WR + T showed a lessened size of testis/body weight ((B): **** $p < 0.0001$) and an increased size of seminal vesicles ((C): *** $p < 0.001$ vs. WR). No alteration of testis or seminal vesicles size was shown in the WR + T + A group (B,C). CTL: control, WR: Wobbler, WR + T: Wobbler + testosterone, WR + T + A: Wobbler + testosterone + anastrozole.

4. Discussion

The present study demonstrated several myelin abnormalities in the spinal cord of mutant WR mice which were mostly ameliorated by T treatment. First, in WR mice, myelin anomalies and low density of CC1+ mature oligodendrocytes coexisted with high levels of proinflammatory factors associated with a low expression of glutamate detoxifying factors. Neuroinflammation and glutamate toxicity were already reported in previous publications [50]. In addition, we investigated the role of T as a potential replacement therapy, considering that male WR mice suffer from hypotestosteronaemia and infertility [10]. We demonstrated that in WR mice, chronic T administration showed myelin-protective and anti-inflammatory effects. These effects may be due to normalization of T and 5 α -DHT to physiological levels although for several parameters, estradiol synthesis plays an important role, as revealed by the use of an aromatase inhibitor. T treatment raised factors such as GS and GLT-1 that favor the glutamate/glutamine cycle, detoxify ammonia and glutamate from the synaptic cleft and also provide energy to neurons via oligodendrocytes and astrocytes [39]. In T-treated WRs, the rise in glutamine pool in the spinal cord, possibly enhances transmission efficacy acting as an energy substrate for axons. Lastly, the regulation of these factors may also depend on estradiol synthesis because WR + T + A lost these protective effects on the glutamate circuit.

Abnormalities of myelin sheaths were demonstrated via different procedures that include low staining of total myelin lipids with LFB and decreased density of myelinated axons assessed by using toluidine-blue-stained semithin sections and electron microscopy [51]. The latter procedure showed aberrant features of myelin with irregular, instead of circularly shaped axonal profiles, and detachment and broken myelin lamellae. Both the g-ratios and regression analysis sustained that myelin abnormalities of empty-silastic-treated WRs could be restored to normal via T treatment.

Because the myelin membrane contains about 15–30% protein of total dry weight, we studied if demyelination and myelin abnormalities of WR spinal cord are accompanied by changes in the expression of three major central myelin proteins. We found lower levels of basal MBP and PLP immunoreactivity in the cervical spinal cord of male WRs without an effect on their mRNAs, similarly to MOG mRNA. The low expression of MBP and PLP and the reduction of mature oligodendrocytes may be the consequence of axonal loss, neurodegeneration and neuroinflammation, findings that require further

investigation. However, normal or even higher expression of myelin protein mRNA may be a compensatory mechanism to counteract the decreased levels of central myelin proteins.

Our past and present investigation of the *WR* mouse also revealed neuroinflammation with increased microglial IBA1+ cells and CD11b mRNA expression in combination with proinflammatory factors including IL18, TLR4, TNF α R₁ and P₂Y₁₂R. These inflammatory mediators originate in activated microglia and astrocytes, which change their role from protection to pathological in *WR* mice [9,52,53]. Accordingly, TLR4 has been found to associate with other inflammatory markers, motoneuron death and low performance in tests of motor behavior [9,29,53]. TLR4 is a component of the NF κ B pathway leading to cytokine production, and in this regard, this receptor induces demyelination and inflammation, as shown in diseases like multiple sclerosis [54]. The colocalization of TNF α and CD11b (a microglia marker) or GFAP (an astrocyte marker) [53,55] supports the hypothesis that pathological microglia and astrocytes of the *WR* disease participate in demyelination. Moreover, we found that IBA1+ cells in the ventrolateral funiculus of the white matter showed an activated morphology in naïve *WR*s which was reduced by T with or without A treatment. IBA1+ microglia of *WR* mice showed a round soma with low branching, a morphology suggesting reactive activation, in contrast with T-treated *WR* mice in which cells with small soma and high branching, typical of quiescent microglia, predominated. Since mRNA for inflammatory factors stayed low after T + A cotreatment, the anti-inflammatory effect of T may depend on AR or ER beta activities on microglial cells. In this regard, it is possible that 5 α -androstane 3 β ,17 β -diol, a reduced metabolite of DHT which is increased in *WR* + T [29], activates ER beta on microglial cells [56].

It is now accepted that glutamate excitotoxicity plays an important role in neurodegeneration of the *WR* mouse. Changes of the enzyme, GS, glutamate-aspartate transporter, GLAST, and GLT-1 are early findings in the spinal cord of 6-day-old postnatal and 5-month-old *WR*s [9]. In *WR*s, this alteration is not confined only to the spinal cord because increased excitatory synaptic transmission has also been found in the hippocampus [57]. Furthermore, ALS patients [58] and SOD^{G93A} presymptomatic transgenic mice also show cerebral cortex hyperexcitability, indicating that disorders of glutamate homeostasis is a common feature of ALS and its animal models [59]. Excitotoxicity follows glutamate binding to AMPA and kainate receptors causing the death of oligodendrocytes and demyelination, a mechanism reported in multiple sclerosis [60,61] that may also apply to neurodegenerative diseases. As already mentioned in the Introduction, androgens stimulate myelinogenesis and remyelination in rodents with demyelination due to cuprizone intoxication, EAE and lysolecithin treatment [18,20,62]. Furthermore, the AR shows an important role in myelin formation in males [63] and has become a promising target to stimulate remyelination [18]. In agreement, the results of the morphological, biochemical and molecular approaches of the present study suggest that T treatment restores myelination in the spinal cord of *WR* mice.

T is the main androgen circulating in mammals and produces androgenic effects upon binding to the AR present in target tissues. However, T is also a pro-hormone, because it can be metabolized to 5 α -dihydrotestosterone, aromatized to estrogens and converted into 5 α -androstane 3 β ,17 β -diol (3 β -diol). Both estradiol and 5 α -androstane 3 β ,17 β -diol bind to the estrogen receptor (ER) [15]. To investigate the role of estradiol in androgen neuroprotection, we administered the aromatase inhibitor, A, to *WR* mice one week before T in order to reduce the level of T aromatization. Previously, we have shown that T administration to male symptomatic *WR*s normalizes the low levels of androgens in the spinal cord to levels similar to those of control mice. However, T administration did not increase estradiol levels but slowed clinical progression of the *WR* disease [10,29]. These observations suggest that the restoration of the physiological levels of androgens is required for neuroprotection. In this work, the administration of an aromatase inhibitor in combination with T halted the improvement of clinical and molecular parameters. These results suggest that estradiol synthesis should also be preserved for the reversal of myelin abnormalities in the *WR* spinal cord. It is also possible that basal estrogen levels are necessary for enabling axonal remyelination in the white matter and preserving cellular antioxidant activity in the spinal

cord. On the other hand, an accelerated clinical deterioration of WR + T + A triggered by the earlier inhibition of aromatase activity might not be discarded. Therefore, both androgens and estrogens are required for neuroprotection in the WR spinal cord. Specifically, after the comparison of results involving WRs receiving T alone or T + A, we found that (a) morphological changes of myelin revealed by LFB and toluidine blue staining, g-ratio analyses, and electron microscopy, (b) myelin proteins at the mRNA (MBP, PLP and MOG) and immunoreactive levels (MBP and PLP), (c) microglia markers (IBA1 and CD11b) as well as (d) glutamatergic parameters (GS, GLT1) were sensitive to the aromatase inhibition by A (Table 2). On the other hand, the decreased expression of inflammatory factors (IL-18, TLR4, TNF α R₁ and P₂Y₁₂R) caused by T were A-insensitive, suggesting more direct anti-inflammatory effects of T (Table 2).

Table 2. Overview of the effects of testosterone and anastrozole on the cervical spinal cord from male *Wobblers*.

	Location	Experimental Groups		
		Male Wobbler	Male Wobbler Testosterone	Male Wobbler Testosterone + Anastrozole
Myelin parameters				
Luxol fast blue	Ventrolateral funiculus	↓ ↓	↑ ↑	↓ ↓
G-ratio	Ventrolateral funiculus	↑	↓	↑
MBP mRNA	Whole CSC	—	↑	↓
MBP-IR	Ventrolateral funiculus	↓	↑	↓
PLP mRNA	Whole CSC	↑ ↑	↑ ↑	↓ ↓
PLP-IR	Ventrolateral funiculus	↓	↑	↓
Inflammatory factors				
CD11b mRNA	Whole CSC	↑ ↑	↓	↑ ↑
IBA1 cell density	Ventral region (Ventral horn + Ventrolateral funiculus)	↑ ↑	↓	↑ ↑
IL-18 mRNA TLR4 mRNA TNF α R ₁ mRNA P ₂ Y ₁₂ R mRNA	Whole CSC	↑ ↑	↓ ↓	↓ ↓
Glutamate metabolism				
GS-IR	Ventral horn	↓ ↓	↑ ↑ ↑	↓ ↓
	Ventrolateral funiculus	↓ ↓	↑ ↑	↓ ↓
GLT-1 mRNA	Whole CSC	↓	↑	↓
GLT-1 IR	Ventral horn	↓ ↓	↑ ↑	↓ ↓

Single arrow represents slight increase (↑) or decrease effects (↓), whereas strong or stronger effects are represented by double (↑↑ or ↓↓) and triple arrows (↑↑↑), respectively.

ALS is a progressive disease of fatal outcome, for which current approved pharmacological treatments enhance the quality of life of or prolong the life of patients for 5–6 months only. Therefore, information produced by preclinical models becomes of utmost importance for their potential translation to clinics. Since ALS patients show high circulating plasma levels of T but low DHT concentration in the cerebrospinal fluid (CSF) [64,65], their normalization may be considered as part of a protective mechanism based on the promyelinating, anti-inflammatory and neuroprotective effects due to T itself or after conversion into reduced derivatives or estrogenic compounds. Here, we showed that T's neuroprotective property improves motor performance, and enhances muscle mass and strength in the WR mouse. Furthermore, at the preclinical level, DHT administration to SOD1 transgenic mouse models reduces muscle atrophy and extends lifespan [66]. On the contrary, treatment with nandrolone, a synthetic androgen, worsens disease progression. These different data warrant further preclinical as well as human studies in ALS patients receiving androgens.

Author Contributions: I.J.E.: Validation, Formal Analysis, Investigation, Data curation, writing—Review & Editing, Visualization. M.M.: Methodology, Validation, Formal Analysis, Investigation, Supervision, Funding Acquisition. C.B.: Investigation, Formal Analysis. M.S.K.: Investigation, writing Review & Editing. P.R. and A.L.: Investigation and Technical assistance. R.G. and M.S.: Discussing results, writing Review & Editing. A.F.D.N.: conceptualization, resources, writing—Original Draft Preparation, writing Review & Editing, Funding Acquisition. M.C.G.D.: Conceptualization, Methodology, Formal Analysis, Investigation, Resources, Data Curation, writing—Original Draft preparation, writing—Review & Editing, Visualization, Supervision, Funding Acquisition. All authors have read and agreed to the published version of the manuscript.

Funding: We thank the financial support of the National Research Council of Argentina [CONICET, PIP 2022–2024 #11220210100091CO], the Ministry of Health and Technology of Argentina (PICT 2019 N° 3292 and PICT 2021 00389), René Barón and Williams Foundations, and the University of Buenos Aires grant [Ubacyt # 20020170100224BA]. These funding sources did not have a role in the collection, analysis, and interpretation of data, in the writing of the report and in the decision to submit the paper for publication. Ivan J. Esperante was the recipient of a CONICET PhD Fellowship, (2021–2026) and Carolina Banzan of a FONCYT PhD Fellowship (2022–2025).

Institutional Review Board Statement: All procedures reported in this paper followed the guide for the Care and Use of Laboratory Animals (Animal Welfare Assurance, NIH certificate granted to our Institute is # F16-00065 A5072-01, and were approved by the Institute's Animal Care and Use Committee). The experiments are reported in accordance with the ARRIVE guidelines (www.nc3rs.org.uk).

Informed Consent Statement: Not applicable.

Data Availability Statement: The data that support the findings of this study are available from the corresponding author upon reasonable request.

Acknowledgments: We greatly thank the collaboration of Juan José Lopez (Facultad de Medicina, UBA) for his help in electron microscopy studies and Juana M. Pasquini (Facultad de Farmacia y Bioquímica, UBA) for the kind donation of the anti-PLP AA3 and CC1 antibodies.

Conflicts of Interest: The authors declare no conflicts of interest.

References

1. Chaudhuri, A. Multiple sclerosis is primarily a neurodegenerative disease. *J. Neural Transm.* **2013**, *120*, 1463–1466. [[CrossRef](#)] [[PubMed](#)]
2. Sandi, D.; Friczka-Nagy, Z.; Bencsik, K.; Vécsei, L. Neurodegeneration in Multiple Sclerosis: Symptoms of Silent Progression, Biomarkers and Neuroprotective Therapy-Kynurenines Are Important Players. *Molecules* **2021**, *26*, 3423. [[CrossRef](#)]
3. Moser, J.M.; Bigini, P.; Schmitt-John, T. The wobbler mouse, an ALS animal model. *Mol. Genet. Genom. MGG* **2013**, *288*, 207–229. [[CrossRef](#)] [[PubMed](#)]
4. Mitsumoto, H.; Ferut, A.L.; Kurahashi, K.; McQuarrie, I.G. Impairment of retrograde axonal transport in wobbler mouse motor neuron disease. *Muscle Nerve* **1990**, *13*, 121–126. [[CrossRef](#)] [[PubMed](#)]
5. Raffaele, S.; Boccazzi, M.; Fumagalli, M. Oligodendrocyte Dysfunction in Amyotrophic Lateral Sclerosis: Mechanisms and Therapeutic Perspectives. *Cells* **2021**, *10*, 565. [[CrossRef](#)] [[PubMed](#)]

6. Monachelli, G.G.; Meyer, M.; Rodríguez, G.E.; Garay, L.I.; Sica, R.E.P.; De Nicola, A.F.; Deniselle, M.C.G. Endogenous progesterone is associated to amyotrophic lateral sclerosis prognostic factors. *Acta Neurol. Scand.* **2011**, *123*, 60–67. [[CrossRef](#)]
7. Meyer, M.; Garay, L.I.; Kruse, M.S.; Lara, A.; Gargiulo-Monachelli, G.; Schumacher, M.; Guennoun, R.; Coirini, H.; De Nicola, A.F.; Deniselle, M.C.G. Protective effects of the neurosteroid allopregnanolone in a mouse model of spontaneous motoneuron degeneration. *J. Steroid Biochem. Mol. Biol.* **2017**, *174*, 201–216. [[CrossRef](#)] [[PubMed](#)]
8. Meyer, M.; Deniselle, M.G.; Garay, L.; Sitruk-Ware, R.; Guennoun, R.; Schumacher, M.; De Nicola, A. The progesterone receptor agonist Nestorone holds back proinflammatory mediators and neuropathology in the wobblers mouse model of motoneuron degeneration. *Neuroscience* **2015**, *308*, 51–63. [[CrossRef](#)] [[PubMed](#)]
9. Meyer, M.; Lima, A.; Deniselle, M.C.G.; De Nicola, A.F. Early Signs of Neuroinflammation in the Postnatal Wobbler Mouse Model of Amyotrophic Lateral Sclerosis. *Cell. Mol. Neurobiol.* **2023**, *43*, 2149–2163. [[CrossRef](#)] [[PubMed](#)]
10. Gonzalez Deniselle, M.C.; Liere, P.; Pianos, A.; Meyer, M.; Aprahamian, F.; Cambourg, A.; Di Giorgio, N.P.; Schumacher, M.; De Nicola, A.F.; Guennoun, R. Steroid Profiling in Male Wobbler Mouse, a Model of Amyotrophic Lateral Sclerosis. *Endocrinology* **2016**, *157*, 4446–4460. [[CrossRef](#)] [[PubMed](#)]
11. Schmitt-John, T.; Drepper, C.; Mußmann, A.; Hahn, P.; Kuhlmann, M.; Thiel, C.; Hafner, M.; Lengeling, A.; Heimann, P.; Jones, J.M.; et al. Mutation of Vps54 causes motor neuron disease and defective spermiogenesis in the wobblers mouse. *Nat. Genet.* **2005**, *37*, 1213–1215. [[CrossRef](#)] [[PubMed](#)]
12. Heimann, P.; Laage, S.; Jockusch, H. Defect of sperm assembly in a neurological mutant of the mouse, wobblers (WR). *Differentiation* **1991**, *47*, 77–83. [[CrossRef](#)]
13. Niebroj-Dobosz, I.; Rafałowska, J.; Fidziańska, A.; Gadamski, R.; Grieb, P. Myelin composition of spinal cord in a model of amyotrophic lateral sclerosis (ALS) in SOD1G93A transgenic rats. *Folia Neuropathol.* **2007**, *45*, 236–241. [[PubMed](#)]
14. Bianchi, V.E.; Rizzi, L.; Bresciani, E.; Omeljaniuk, R.J.; Torsello, A. Androgen Therapy in Neurodegenerative Diseases. *J. Endocr. Soc.* **2020**, *4*, bvaa120. [[CrossRef](#)] [[PubMed](#)]
15. Schumacher, M.; Ghomari, A.; Mattern, C.; Bougnères, P.; Traiffort, E. Testosterone and Myelin Regeneration in the Central Nervous System. *Androg. Clin. Res. Ther.* **2021**, *2*, 231–251. [[CrossRef](#)]
16. Gaignard, P.; Liere, P.; Théron, P.; Schumacher, M.; Slama, A.; Guennoun, R. Role of Sex Hormones on Brain Mitochondrial Function, with Special Reference to Aging and Neurodegenerative Diseases. *Front. Aging Neurosci.* **2017**, *9*, 406. [[CrossRef](#)] [[PubMed](#)]
17. Pesaresi, M.; Soon-Shiong, R.; French, L.; Kaplan, D.; Miller, F.; Paus, T. Axon diameter and axonal transport: In vivo and in vitro effects of androgens. *Neuroimage* **2015**, *115*, 191–201. [[CrossRef](#)] [[PubMed](#)]
18. Hussain, R.; Ghomari, A.M.; Bielecki, B.; Steibel, J.; Boehm, N.; Liere, P.; Macklin, W.B.; Kumar, N.; Habert, R.; Mhaouty-Kodja, S.; et al. The neural androgen receptor: A therapeutic target for myelin repair in chronic demyelination. *Brain* **2013**, *136*, 132–146. [[CrossRef](#)] [[PubMed](#)]
19. Bielecki, B.; Mattern, C.; Ghomari, A.M.; Javaid, S.; Smietanka, K.; Ghanem, C.A.; Mhaouty-Kodja, S.; Ghandour, M.S.; Baulieu, E.-E.; Franklin, R.J.M.; et al. Unexpected central role of the androgen receptor in the spontaneous regeneration of myelin. *Proc. Natl. Acad. Sci. USA* **2016**, *113*, 14829–14834. [[CrossRef](#)] [[PubMed](#)]
20. Ghomari, A.M.; Ghanem, C.A.; Asbelaoui, N.; Schumacher, M.; Hussain, R. Roles of Progesterone, Testosterone and Their Nuclear Receptors in Central Nervous System Myelination and Remyelination. *Int. J. Mol. Sci.* **2020**, *21*, 3163. [[CrossRef](#)] [[PubMed](#)]
21. Weiner, L.P. Possible role of androgen receptors in amyotrophic lateral sclerosis: A hypothesis. *Arch. Neurol.* **1980**, *37*, 129–131. [[CrossRef](#)] [[PubMed](#)]
22. Cappello, V.; Vezzoli, E.; Righi, M.; Fossati, M.; Mariotti, R.; Crespi, A.; Patruno, M.; Bentivoglio, M.; Pietrini, G.; Francolini, M. Analysis of neuromuscular junctions and effects of anabolic steroid administration in the SOD1G93A mouse model of ALS. *Mol. Cell. Neurosci.* **2012**, *51*, 12–21. [[CrossRef](#)] [[PubMed](#)]
23. Galbiati, M.; Onesto, E.; Zito, A.; Crippa, V.; Rusmini, P.; Mariotti, R.; Bentivoglio, M.; Bendotti, C.; Poletti, A. The anabolic/androgenic steroid nandrolone exacerbates gene expression modifications induced by mutant SOD1 in muscles of mice models of amyotrophic lateral sclerosis. *Pharmacol. Res.* **2012**, *65*, 221–230. [[CrossRef](#)] [[PubMed](#)]
24. Kaspar, B.K.; Frost, L.M.; Christian, L.; Umapathi, P.; Gage, F.H. Synergy of insulin-like growth factor-1 and exercise in amyotrophic lateral sclerosis. *Ann. Neurol.* **2005**, *57*, 649–655. [[CrossRef](#)] [[PubMed](#)]
25. Zahaf, A.; Kassoussi, A.; Hutteau-Hamel, T.; Mellouk, A.; Marie, C.; Zoupi, L.; Tsouki, F.; Mattern, C.; Bobé, P.; Schumacher, M.; et al. Androgens show sex-dependent differences in myelination in immune and non-immune murine models of CNS demyelination. *Nat. Commun.* **2023**, *14*, 1592. [[CrossRef](#)] [[PubMed](#)]
26. Magnaghi, V.; Ballabio, M.; Gonzalez, L.C.; Leonelli, E.; Motta, M.; Melcangi, R.C. The synthesis of glycoprotein Po and peripheral myelin protein 22 in sciatic nerve of male rats is modulated by testosterone metabolites. *Brain Res. Mol. Brain Res.* **2004**, *126*, 67–73. [[CrossRef](#)] [[PubMed](#)]
27. Roglio, I.; Bianchi, R.; Giatti, S.; Cavaletti, G.; Caruso, D.; Scurati, S.; Crippa, D.; Garcia-Segura, L.M.; Camozzi, F.; Lauria, G.; et al. Testosterone derivatives are neuroprotective agents in experimental diabetic neuropathy. *Cell. Mol. Life Sci. CMLS* **2007**, *64*, 1158–1168. [[CrossRef](#)] [[PubMed](#)]
28. Melcangi, R.; Ballabio, M.; Cavarretta, I.; Gonzalez, L.; Leonelli, E.; Veiga, S.; Martini, L.; Magnaghi, V. Effects of neuroactive steroids on myelin of peripheral nervous system. *J. Steroid Biochem. Mol. Biol.* **2003**, *85*, 323–327. [[CrossRef](#)] [[PubMed](#)]

29. Lara, A.; Esperante, I.; Meyer, M.; Liere, P.; Di Giorgio, N.; Schumacher, M.; Guennoun, R.; Gargiulo-Monachelli, G.; De Nicola, A.F.; Deniselle, M.C.G. Neuroprotective Effects of Testosterone in Male Wobbler Mouse, a Model of Amyotrophic Lateral Sclerosis. *Mol. Neurobiol.* **2021**, *58*, 2088–2106. [[CrossRef](#)] [[PubMed](#)]
30. Meyer, M.; Deniselle, M.C.G.; Garay, L.I.; Monachelli, G.G.; Lima, A.; Roig, P.; Guennoun, R.; Schumacher, M.; De Nicola, A.F. Stage Dependent Effects of Progesterone on Motoneurons and Glial Cells of Wobbler Mouse Spinal Cord Degeneration. *Cell. Mol. Neurobiol.* **2010**, *30*, 123–135. [[CrossRef](#)] [[PubMed](#)]
31. Gonzalez Deniselle, M.C. Progesterone neuroprotection in the Wobbler mouse, a genetic model of spinal cord motor neuron disease. *Neurobiol. Dis.* **2002**, *11*, 457–468. [[CrossRef](#)] [[PubMed](#)]
32. Gargiulo-Monachelli, G.; Meyer, M.; Lara, A.; Garay, L.; Lima, A.; Roig, P.; De Nicola, A.F.; Deniselle, M.C.G. Comparative effects of progesterone and the synthetic progestin norethindrone on neuroprotection in a model of spontaneous motoneuron degeneration. *J. Steroid Biochem. Mol. Biol.* **2019**, *192*, 105385. [[CrossRef](#)] [[PubMed](#)]
33. Chomiak, T.; Hu, B. What is the optimal value of the g-ratio for myelinated fibers in the rat CNS? A theoretical approach. *PLoS ONE* **2009**, *4*, e7754. [[CrossRef](#)] [[PubMed](#)]
34. Kaiser, T.; Allen, H.M.; Kwon, O.; Barak, B.; Wang, J.; He, Z.; Jiang, M.; Feng, G. MyelTracer: A Semi-Automated Software for Myelin g-Ratio Quantification. *eNeuro* **2021**, *8*, eneuro.0558-20.2021. [[CrossRef](#)] [[PubMed](#)]
35. Dillenburg, A.; Ireland, G.; Holloway, R.K.; Davies, C.L.; Evans, F.L.; Swire, M.; Bechler, M.E.; Soong, D.; Yuen, T.J.; Su, G.H.; et al. Activin receptors regulate the oligodendrocyte lineage in health and disease. *Acta Neuropathol.* **2018**, *135*, 887–906. [[CrossRef](#)] [[PubMed](#)]
36. Kim, J.H.; Budde, M.D.; Liang, H.-F.; Klein, R.S.; Russell, J.H.; Cross, A.H.; Song, S.-K. Detecting axon damage in spinal cord from a mouse model of multiple sclerosis. *Neurobiol. Dis.* **2006**, *21*, 626–632. [[CrossRef](#)] [[PubMed](#)]
37. Garay, L.; Tüngler, V.; Deniselle, M.; Lima, A.; Roig, P.; De Nicola, A. Progesterone attenuates demyelination and microglial reaction in the lysolecithin-injured spinal cord. *Neuroscience* **2011**, *192*, 588–597. [[CrossRef](#)] [[PubMed](#)]
38. Labombarda, F.; Gonzalez, S.; Deniselle, M.C.G.; Garay, L.; Guennoun, R.; Schumacher, M.; De Nicola, A.F. Progesterone increases the expression of myelin basic protein and the number of cells showing NG2 immunostaining in the lesioned spinal cord. *J. Neurotrauma* **2006**, *23*, 181–192. [[CrossRef](#)] [[PubMed](#)]
39. Xin, W.; Mironova, Y.A.; Shen, H.; Marino, R.A.; Waisman, A.; Lamers, W.H.; Bergles, D.E.; Bonci, A. Oligodendrocytes Support Neuronal Glutamatergic Transmission via Expression of Glutamine Synthetase. *Cell Rep.* **2019**, *27*, 2262–2271.e5. [[CrossRef](#)] [[PubMed](#)]
40. Ben Haim, L.; Schirmer, L.; Zulji, A.; Sabeur, K.; Turet, B.; Ribon, M.; Chang, S.; Lamers, W.H.; Boillée, S.; Chaumeil, M.M.; et al. Evidence for glutamine synthetase function in mouse spinal cord oligodendrocytes. *Glia* **2021**, *69*, 2812–2827. [[CrossRef](#)]
41. Leicaj, M.L.; Pasquini, L.A.; Lima, A.; Deniselle, M.G.; Pasquini, J.M.; De Nicola, A.F.; Garay, L.I. Changes in neurosteroidogenesis during demyelination and remyelination in cuprizone-treated mice. *J. Neuroendocr.* **2018**, *30*, e12649. [[CrossRef](#)] [[PubMed](#)]
42. Meyer, M.; Lara, A.; Hunt, H.; Belanoff, J.; de Kloet, E.R.; Deniselle, M.C.G.; De Nicola, A.F. The Selective Glucocorticoid Receptor Modulator Cort 113176 Reduces Neurodegeneration and Neuroinflammation in Wobbler Mice Spinal Cord. *Neuroscience* **2018**, *384*, 384–396. [[CrossRef](#)] [[PubMed](#)]
43. Livak, K.J.; Schmittgen, T.D. Analysis of relative gene expression data using real-time quantitative PCR and the $2^{-\Delta\Delta CT}$ Method. *Methods* **2001**, *25*, 402–408. [[CrossRef](#)] [[PubMed](#)]
44. Mitsumoto, H.; Ikeda, K.; Holmlund, T.; Greene, T.; Cedarbaum, J.M.; Wong, V.; Lindsay, R.M. The effects of ciliary neurotrophic factor on motor dysfunction in wobbler mouse motor neuron disease. *Ann. Neurol.* **1994**, *36*, 142–148. [[CrossRef](#)] [[PubMed](#)]
45. Krieger, C.; Perry, T.L.; Hansen, S.; Mitsumoto, H.; Honoré, T. Excitatory Amino Acid Receptor Antagonist in Murine Motoneuron Disease (The Wobbler Mouse). *Can. J. Neurol. Sci.* **1992**, *19*, 462–465. [[CrossRef](#)] [[PubMed](#)]
46. Marzan, D.E.; Brügger-Verdon, V.; West, B.L.; Liddelow, S.; Samanta, J.; Salzer, J.L. Activated microglia drive demyelination via CSF1R signaling. *Glia* **2021**, *69*, 1583–1604. [[CrossRef](#)] [[PubMed](#)]
47. Traiffort, E.; Morisset-Lopez, S.; Moussaed, M.; Zahaf, A. Defective Oligodendroglial Lineage and Demyelination in Amyotrophic Lateral Sclerosis. *Int. J. Mol. Sci.* **2021**, *22*, 3426. [[CrossRef](#)] [[PubMed](#)]
48. Blondet, B.; Hantaz-Ambroise, D.; Aït-Ikhlef, A.; Cambier, D.; Murawsky, M.; Rieger, F. Astrocytosis in wobbler mouse spinal cord involves a population of astrocytes which is glutamine synthetase-negative. *Neurosci. Lett.* **1995**, *183*, 179–182. [[CrossRef](#)] [[PubMed](#)]
49. Diana, V.; Ottolina, A.; Botti, F.; Fumagalli, E.; Calcagno, E.; De Paola, M.; Cagnotto, A.; Invernici, G.; Parati, E.; Curti, D.; et al. Neural precursor-derived astrocytes of wobbler mice induce apoptotic death of motor neurons through reduced glutamate uptake. *Exp. Neurol.* **2010**, *225*, 163–172. [[CrossRef](#)] [[PubMed](#)]
50. Meyer, M.; Kruse, M.S.; Garay, L.; Lima, A.; Roig, P.; Hunt, H.; Belanoff, J.; de Kloet, E.R.; Deniselle, M.C.G.; De Nicola, A.F. Long-term effects of the glucocorticoid receptor modulator CORT113176 in murine motoneuron degeneration. *Brain Res.* **2020**, *1727*, 146551. [[CrossRef](#)] [[PubMed](#)]
51. Ohno, N.; Ikenaka, K. Axonal and neuronal degeneration in myelin diseases. *Neurosci. Res.* **2019**, *139*, 48–57. [[CrossRef](#)] [[PubMed](#)]
52. Bigini, P.; Diana, V.; Barbera, S.; Fumagalli, E.; Micotti, E.; Sitia, L.; Paladini, A.; Bisighini, C.; De Grada, L.; Coloca, L.; et al. Longitudinal tracking of human fetal cells labeled with super paramagnetic iron oxide nanoparticles in the brain of mice with motor neuron disease. *PLoS ONE* **2012**, *7*, e32326. [[CrossRef](#)] [[PubMed](#)]

53. De Paola, M.; Mariani, A.; Bigini, P.; Peviani, M.; Ferrara, G.; Molteni, M.; Gemma, S.; Veglianese, P.; Castellaneta, V.; Boldrin, V.; et al. Neuroprotective effects of toll-like receptor 4 antagonism in spinal cord cultures and in a mouse model of motor neuron degeneration. *Mol. Med.* **2012**, *18*, 971–981. [[CrossRef](#)] [[PubMed](#)]
54. Li, H.; Liu, S.; Han, J.; Li, S.; Gao, X.; Wang, M.; Zhu, J.; Jin, T. Role of Toll-Like Receptors in Neuroimmune Diseases: Therapeutic Targets and Problems. *Front. Immunol.* **2021**, *12*, 777606. [[CrossRef](#)] [[PubMed](#)]
55. Garay, L.; Deniselle, M.G.; Brocca, M.; Lima, A.; Roig, P.; De Nicola, A. Progesterone down-regulates spinal cord inflammatory mediators and increases myelination in experimental autoimmune encephalomyelitis. *Neuroscience* **2012**, *226*, 40–50. [[CrossRef](#)] [[PubMed](#)]
56. Yılmaz, C.; Karali, K.; Fodelianaki, G.; Gravanis, A.; Chavakis, T.; Charalampopoulos, I.; Alexaki, V.I. Neurosteroids as regulators of neuroinflammation. *Front. Neuroendocrinol.* **2019**, *55*, 100788. [[CrossRef](#)] [[PubMed](#)]
57. Thielsen, K.D.; Moser, J.M.; Schmitt-John, T.; Jensen, M.S.; Jensen, K.; Holm, M.M. The Wobbler Mouse Model of Amyotrophic Lateral Sclerosis (ALS) Displays Hippocampal Hyperexcitability, and Reduced Number of Interneurons, but No Presynaptic Vesicle Release Impairments. *PLoS ONE* **2013**, *8*, e82767. [[CrossRef](#)] [[PubMed](#)]
58. Timmins, H.C.; Vucic, S.; Kiernan, M.C. Cortical hyperexcitability in amyotrophic lateral sclerosis: From pathogenesis to diagnosis. *Curr. Opin. Neurol.* **2023**, *36*, 353–359. [[CrossRef](#)]
59. Saba, L.; Viscomi, M.T.; Caioli, S.; Pignataro, A.; Bisicchia, E.; Pieri, M.; Molinari, M.; Ammassari-Teule, M.; Zona, C. Altered Functionality, Morphology, and Vesicular Glutamate Transporter Expression of Cortical Motor Neurons from a Presymptomatic Mouse Model of Amyotrophic Lateral Sclerosis. *Cereb. Cortex* **2016**, *26*, 1512–1528. [[CrossRef](#)] [[PubMed](#)]
60. Macrez, R.; Stys, P.K.; Vivien, D.; A Lipton, S.; Docagne, F. Mechanisms of glutamate toxicity in multiple sclerosis: Biomarker and therapeutic opportunities. *Lancet Neurol.* **2016**, *15*, 1089–1102. [[CrossRef](#)] [[PubMed](#)]
61. Matute, C.; Alberdi, E.; Domercq, M.; Pérez-Cerdá, F.; Pérez-Samartín, A.; Sánchez-Gómez, M.V. The link between excitotoxic oligodendroglial death and demyelinating diseases. *Trends Neurosci.* **2001**, *24*, 224–230. [[CrossRef](#)] [[PubMed](#)]
62. Laouarem, Y.; Kassoussi, A.; Zahaf, A.; Hutteau-Hamel, T.; Mellouk, A.; Bobé, P.; Mattern, C.; Schumacher, M.; Traiffort, E. Functional cooperation of the hedgehog and androgen signaling pathways during developmental and repairing myelination. *Glia* **2021**, *69*, 1369–1392. [[CrossRef](#)] [[PubMed](#)]
63. Ghanem, C.A.; Degerny, C.; Hussain, R.; Liere, P.; Pianos, A.; Tourpin, S.; Habert, R.; Macklin, W.B.; Schumacher, M.; Ghomari, A.M. Long-lasting masculinizing effects of postnatal androgens on myelin governed by the brain androgen receptor. *PLoS Genet.* **2017**, *13*, e1007049. [[CrossRef](#)] [[PubMed](#)]
64. Sawal, N.; Kaur, J.; Kaur, K.; Gombar, S. Dihydrotestosterone in Amyotrophic lateral sclerosis-The missing link? *Brain Behav.* **2020**, *10*, e01645. [[CrossRef](#)] [[PubMed](#)]
65. Gargiulo-Monachelli, G.M.; Sivori, M.; Meyer, M.; Sica, R.E.P.; De Nicola, A.F.; Gonzalez-Deniselle, M.C. Circulating Gonadal and Adrenal Steroids in Amyotrophic Lateral Sclerosis: Possible Markers of Susceptibility and Outcome. *Horm. Metab. Res.* **2014**, *46*, 433–439. [[CrossRef](#)] [[PubMed](#)]
66. Scaricamazza, S.; Salvatori, I.; Ferri, A.; Valle, C. Skeletal Muscle in ALS: An Unappreciated Therapeutic Opportunity? *Cells* **2021**, *10*, 525. [[CrossRef](#)] [[PubMed](#)]

Disclaimer/Publisher’s Note: The statements, opinions and data contained in all publications are solely those of the individual author(s) and contributor(s) and not of MDPI and/or the editor(s). MDPI and/or the editor(s) disclaim responsibility for any injury to people or property resulting from any ideas, methods, instructions or products referred to in the content.